ISSN 0736-5306

SCIENCE OF TSUNAMI HAZARDS

The International Journal of The Tsunami Society

Volume 12 Number 2 1994

OBJECTIVE: **The Tsunami Society** publishes this journal to increase and disseminate knowledge about tsunamis and their hazards.

DISCLAIMER: Although these articles have been technically reviewed by peers, **The Tsunami Society** is not responsible for the veractiy of any statement, opinion or consequences.

Submit manuscripts of articles, notes or letters to the Editor. If an article is accepted for publication the author(s) must submit a camera ready manuscript in the journal format. A voluntary $50.00 page charge ($35.00 for Tsunami Society Members) will include 50 reprints.

SUBSCRIPTION INFORMATION: Price per copy $20.00 USA

ISSN 0736-5306

Published by The Tsunami Society, P. O. Box 25218, Honolulu, HI 96825 , USA

MOMENT RELEASE OF THE 1992 FLORES ISLAND EARTHQUAKE INFERRED FROM TSUNAMI AND TELESEISMIC DATA

Fumihiko Imamura

School of Civil Engineering, Asian Institute of Technology, G.P.O.Box 2754, Bangkok 10501, Thailand

Masayuki Kikuchi

Department of Physics, Yokohama City University, Yokohama 236, Japan

ABSTRACT

The Flores Island, Indonesia, earthquake of 1992 occurred in the back arc region of the transition from the Sunda to Banda trenches and generated a large tsunami. In order to investigate the moment release of this event, we analyzed tsunami and crustal-motion data obtained by the field survey, as well as teleseismic data observed at the global seismograph network. From the analysis of tsunami data, we inferred a composite fault model consisting of two fault segments with a common mechanism: (strike,dip,slip)=(61°,32°,64°) but different slip values: 3.2 m and 9.6 m. The depth extent of the fault plane is rather shallow, ranging from 3 to 15 km. This composite fault model is consistent with the measured crustal movement. Body wave analyses also indicate that the moment release occurred mainly in a shallow region, and the slip in the eastern portion of the region was larger than in the western portion.

INTRODUCTION

On December 12,1992, at 13:30 (local time), a large earthquake of magnitude Ms=7.5 struck the eastern part of Flores Island in the back arc region of the eastern Sunda and western Banda of Indonesia and generated a large tsunami. The epicenter is located about 1,800 km east of Jakarta at (8.48°S,121.90°E) determined by United State Geological Survey [USGS, 1993] shown in Fig.1. There were about 1,800 deaths and 2,100 injuries, approximately 50% of which were attributed to the tsunami [Tsuji et al.,1993].

Sunarjo (1993) studied historical destructive earthquakes recorded by the Meteorological and Geophysical Agency (MGA) of Indonesia, and reported that the Flores area had been struck by five destructive earthquakes since the end of 19th century. These occurred in 1938, 1961, 1982 (2 times) and 1987. The epicenters of these 5 earthquakes are shown in Fig.1 with the epicenter of this latest earthquake. Before the 1992 event, tsunami were generated by only 2 of these 5 earthquakes, and with no severe damage being reported.

In this paper, we study the rupture process of the 1992 event by analyzing not only teleseismic data but also field survey data such as tsunami heights and crustal movement, measured by the International Tsunami Survey Team [Tsuji et al., 1993; Yeh et al., 1993].

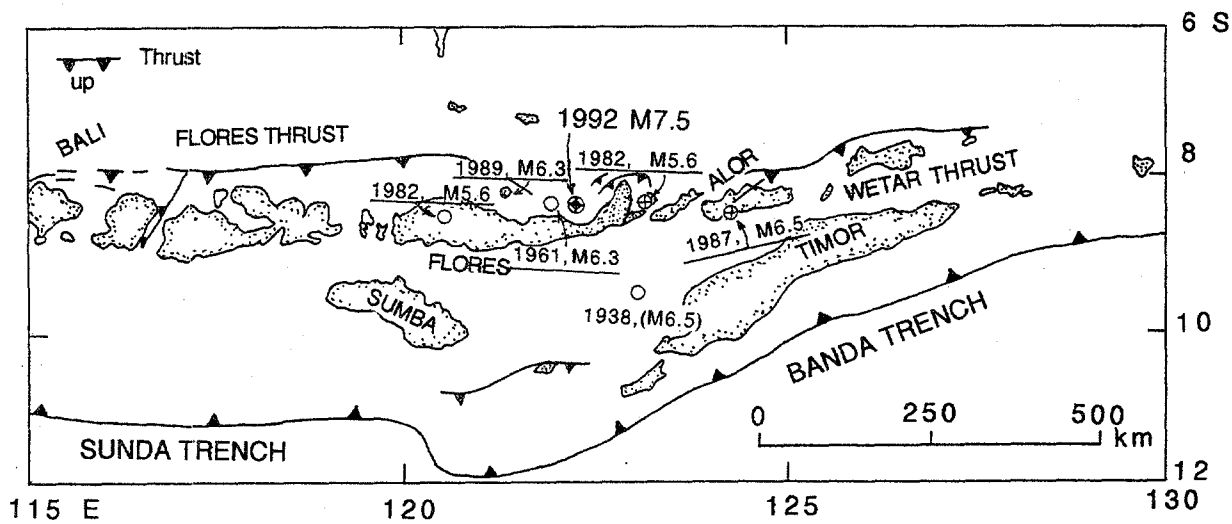

Figure 1: Tectonic and earthquake epicenter map of the eastern Sunda arc, from Bali to Wetar. Flores Island is located in the back arc of the eastern Sunda and western Banda thrusts. There were 5 earthquakes in the Flores area during the last 100 years. Open circles denote earthquakes without tsunami and circles with crosses denote earthquakes with tsunami.

PRELIMINARY SEISMIC WAVE ANALYSIS

Figure 2 shows an overview of the eastern part of Flores Island and the source region of the 19 92 Flores Island earthquake. The largest black circle in the figure indicates the main shock epicenter determined by USGS, while the star indicates the centroid location (8.36°S,122.37°E) of a quick Centroid Momentum Tensor (CMT) solution (event file M121292Y) given by Harvard University. The length of the aftershock area is about 100km. The best-fit double-couple of this
CMT solution is a thrust fault with (strik, dip, slip) = (61°,32°,64°) or (272°,61°,106°). The USGS(1993) moment tensor mechanism has a similar focal mechanism of (65°, 47°, 61°) or (284°, 50°, 118°). These mechanism solutions indicate N-S compression, which is consistent with the tectonics estimated by previous studies (e.g. Fitch, 1972; Silver et al., 1983; McCaffrey and Nabelek, 1984). On the other hand, the quantitative aspect of the 1992 earthquake source is still ambiguous. For example, the scalar moment of the Harvard CMT is Mo=6.4x10^{27} dyne-cm, while that of USGS(1993) is Mo=1.4x10^{27} dyne-cm. Moreover, the centroid depth estimation varies from 20 to 50 km. As shall be discussed later, the tsunami and crustal deformation data combined with teleseismic body wave data would give good constraints on the quantitative estimation of the above parameters.

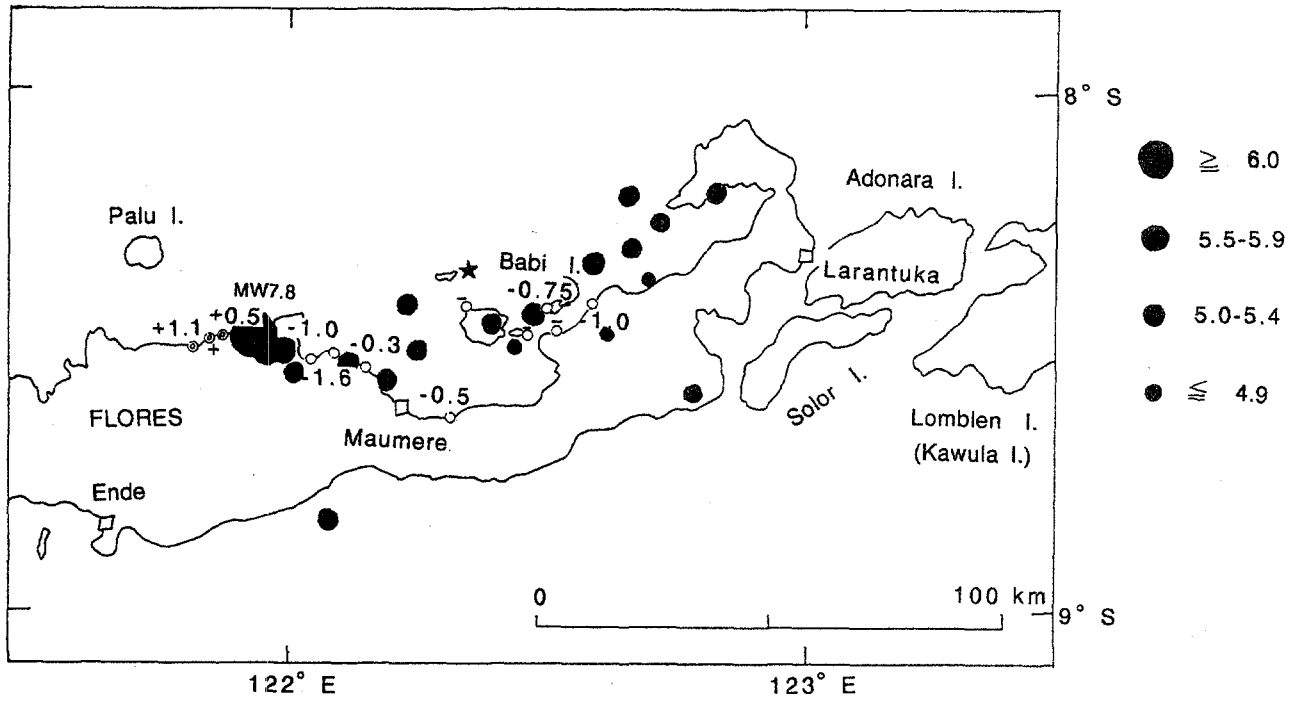

Figure 2: Aftershock distribution within 1 day of the mainshock [USGS, 1993] and the main shock [Harvard CMT solution]; and vertical crustal movement in meters [Tsuji et al.,1993] in the eastern part of Flores Island.

TSUNAMI DATA AND ANALYSIS

The International Tsunami Survey Team (ITST) conducted its field survey on the eastern part of Flores Island, gathering tsunami and seismic data from December 29, 1992 to January 5, 1993 [Yeh et al., 1993]. Figure 3 shows the measured values of the tsunami heights at each location. A general trend of increasing wave height from west to east in this region was clearly noticed. Values ranged from 2 to 5 m in the western region, from 3 to 11 m between Babi Island and the head of Hading Bay, and from 12 to 26 m on the northeast peninsula.

Numerical simulation of tsunami propagation [Imamura et al., 1993] was carried out for three models shown in Table 1. Model-A corresponds to the quick Harvard CMT solution. Taking into account the tectonics of this region, especially the Flores thrust [Hamilton,1988], a shallow dip thrust fault with (strike,dip, slip)= (61°,32°,64°) is preferable to the other Harvard CMT solution for the 1992 Flores earthquake. From the distribution of aftershocks in Fig.2, it was assumed that the fault plane was 100 km long and 50 km wide. From the Harvard CMT moment, $Mo=6.4\times10^{27}$ dyne-cm, we obtain an average dislocation of 3.2 m using the rigidity of 4.0×10^{11} dyne/cm^2. The computational conditions are summaried in Table 2.

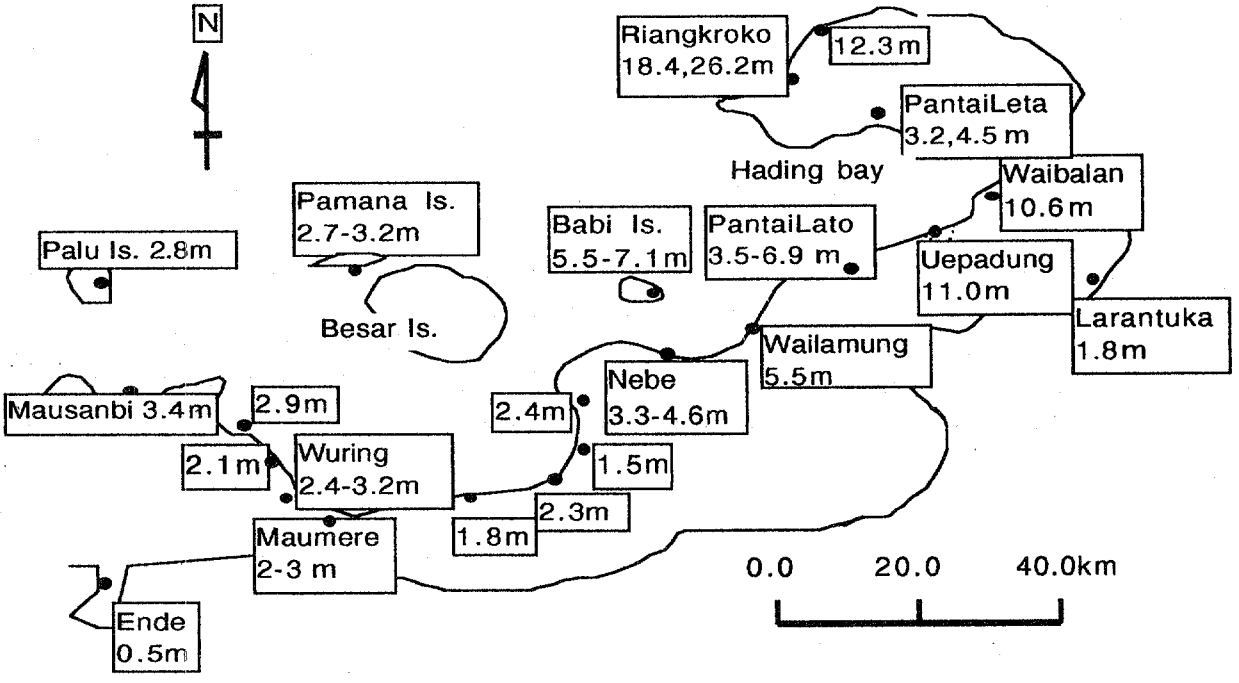

Figure 3: Measured tsunami run-up height in meter on eastern Flores Island [Tsuji et al., 1993]. A general trend of increasing wave height from west to east in this region is evident.

Table 1 Fault parameter for numerical analyses of the 1992 Flores earthquake

	Mo ($\times 10^{27}$dyn-cm)	Depth (km)	Strike (deg)	Dip (deg)	Slip (deg)	Length (km)	Width (km)	Dislocation (m)
Model-A	6.4	15	61	32	64	100	50	3.2
Model-B								
(East)	6.4	15	61	32	64	50	25	9.6
(West)		15	61	32	64	50	25	3.2
Model-C								
(East)	6.4	3	61	32	64	50	25	9.6
(West)		3	61	32	64	50	25	3.2

Table 2 Computational conditions

Governing Equation	Shallow water theory (nonlinear long wave theory)
Spatial grid size	300 m
Time step	1 sec
B.C. of coastal line	Perfect reflection condition (vertical wall)
Reproduction time	1 hour

Figure 4 shows a comparison between the measured tsunami run-up heights and those estimated from Model-A. The result shows that this fault model cannot sufficiently reproduce the distribution of the measured tsunami heights along the coastline of eastern Flores Island. The discrepancy is not likely to be caused by the local effects of such as coastal geometry, because the variation of tsunami run-up heights shown by error-bars in Fig.4 is much smaller than the discrepancy.

In order to fit the observed large tsunamis in the eastern region, we modified the tsunami source model, so that the fault motion in the northeast region has a larger slip value. Keeping the seismic moment fixed at 6.4×10^{27} dyne-cm, we constructed a fault model (Model-B) with two segments, one in the southwest having a slip value of 3.2 m and the other in the northeast having a slip of 9.6 m. Both segments have the same fault dimensions (50 km long and 25 km wide) and the upper side of the fault plane is placed at a depth of h=15 km, so that the centroid depth coincides with the Harvard CMT. The results for Model-B are presented in Fig.4, indicating that the composite fault model is more accurate than the single fault model (Model-A). It reproduces the distribution of tsunami heights, even in the northeast region with the exception of Uepandung, Waibalan and Riangkroko.

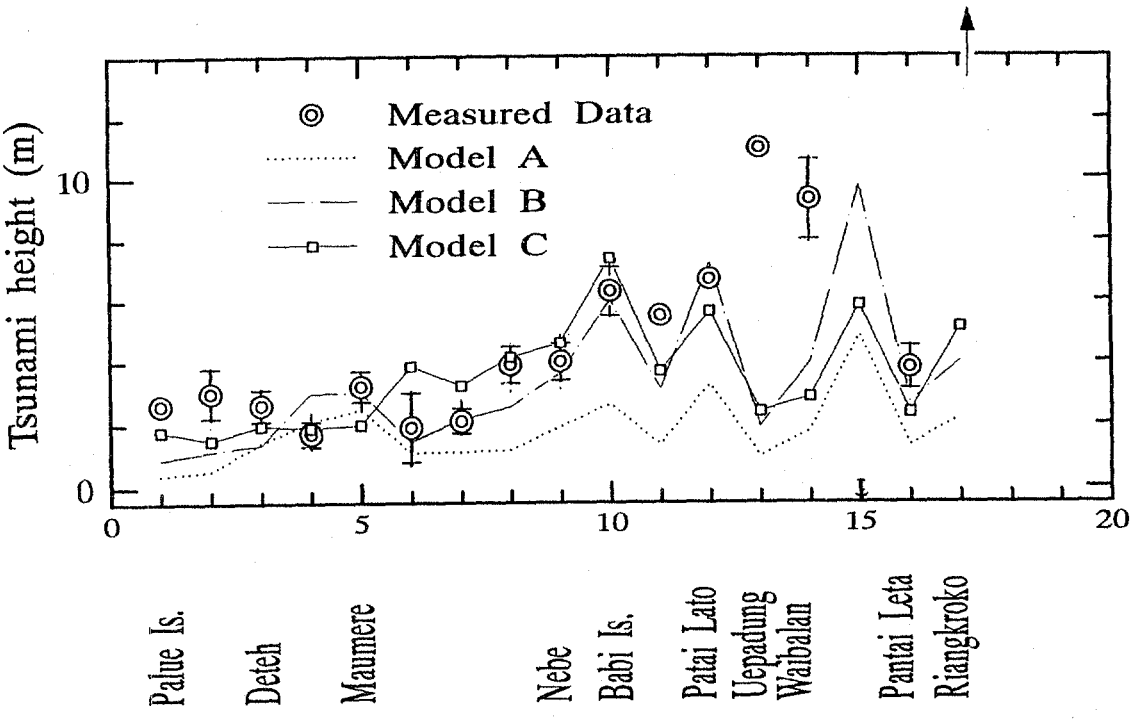

Figure 4: Comparison between measured and computed tsunami heights along the coast of eastern Flores Island. The computed tsunami heights without run-up condition are the maximum water levels along shore lines. Horizontal axis shows the number of observation points from west to east. The upward-pointing arrow indicates that the measured tsunami heights at Riangkroko is more than 15 m (see Fig.3). The error-bars for the measured data indicate the variance of data at the same area/point. The results for Model-B and Model-C with composite fault model are better than that of Model-A with a single fault model. The measured height at Uepadung, Waibalan and Riangkroko might be influenced by a land slide or local effect.

In Uepandung and Waibalan, a local tsunami might be generated due to landsliding as shown by the crosses in Fig.3. Multiple massive subaqueous slumps were observed along the south shore of Hading Bay. On the shoreline near Uepandung and Waibalan, the landslide is approximately 150 m wide, standing 2 km along the shoreline [Yeh et al., 1993]. The wave period of local tsunami generated by this size of landslide would be so short that only a small area would be subjected to a large tsunami height. In order to confirm this, a new wave generation model due to landslide needs to be developed. At this time, however, we cannot carry out the numerical simulation for tsunami due to the landslide to compare the measured data, because of the lack of information about it on the field.

On the other hand, not large landslide but small ons was observed at Riangkroko, although the maximum run-up height was 26 m. The average height based on four different tsunami marks was 19.6 m. Considering the reason why such large tsunami heights were observed, it should be notice here that the northwest side of Riangkroko village faces the Flores Sea where the sea bottom steeply slopes toward west. The large run-up height at Riangkroko might be related to the

wave propagation on a steep slope and the run-up process on land.

In order to investigate the influence of fault depth on the computed results, we constructed an additional model (Model-C) with two fault segments at a shallower depth, the upper side locating at h=3 km. It is difficult to judge whether Model-B or Model-C provide a better fit of the measured data in Fig.4. Therefore, in the following section, the fault depth will be discussed by comparing the crustal deformations measured in Flores Island.

CRUSTAL MOVEMENT

Fault motion causes crustal deformation, which can be estimated from the sea level change associated with an earthquake. Since there was no tidal station on Flores Island, we conducted interviews to determine the sea level change before and after the earthquake. We took care not to include the ground level changes caused by liquefaction. Thus we got the information on the ground movement. The result is shown in Fig. 5, where the subsidence of ground is observed from Mausanbi to Wailamung in the eastern Flores Island. This subsidence is consistent with the observation at Maumere by the National Geodetic Network of Global Positioning System (GPS), -150.7 mm [Gonzalez et al., 1993], and also with the result of Model-C as shown in Fig.5.

The data of crustal movement supports not Model-B but Model-C. The area of positive vertical ground motion in Model-B is wider than that observed and the calculated value at Maumere in Model-B is positive, which is the opposite of the observed value. Thus, we can conclude that Model-C can best represents the observed data among three models.

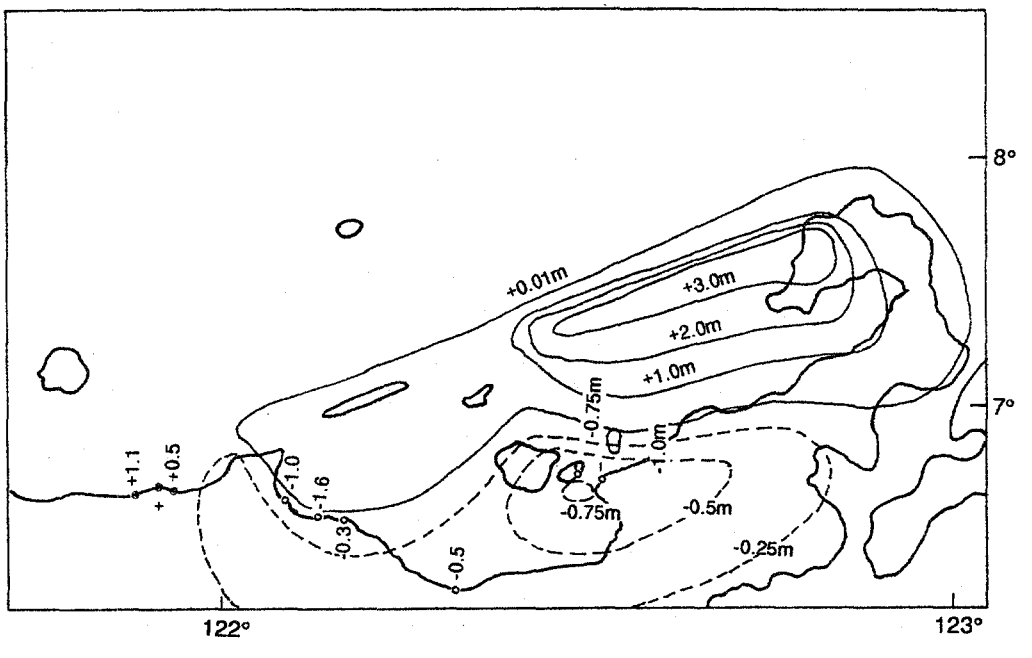

Figure 5: Vertical displacement of ground estimated from Model-C. ○ and ◎ indicate the position of the observation site with negative and positive values, respectively. The estimated data are consistent with observed data in the whole region except for Mausanbi (see Fig.3).

BODY WAVES ANALYSIS

From the IRIS broadband network, we chose five stations (MAJO, COL, RAR, SNZO and TATO). Inspecting the quality of records, we picked vertical components of P waves at 5 stations and SH waves at 2 stations for the source inversion as shown in Fig.6(d), and applied the iterative deconvolution technique developed by Kikuchi and Fukao (1985) for a fixed mechanism. For Green's functions, we assumed a stratified structure consisting of four layers: 1km-thick water layer, 2 km-thick sedimentary layer, 7 km-thick oceanic crust, and a semi-infinite mantle.

After some trial and error, we obtained a sequence of 8 subevents, each having a duration of 9 seconds. The total seismic moment is Mo=5.3×10^{27} dyne-cm, and the moment rate function is shown in Fig.6(a). The figure shows three subevent-clusters as denoted by A, B and C. The total Mo value is in good agreement with the Harvard CMT solution. The best-fit fault mechanism is shown in Fig.6(b). This mechanism is nearly the same as the one given by the USGS (1993) and by Harvard CMT solution.

The distribution of subevents on the fault plane is shown in Fig.6(c). The spatial resolution is rather poor because of the limited azimuthal coverage of the stations, but the depth extent is well constrained because of the depth phases contained in the waveforms. We compared the variance reduction for various depth ranges. We found that the residual error was minimized for the grid scheme with a depth extent between 4 and 13 km. This strongly supports the evidence that the moment release occurred mainly in a very shallow region around 10 km. The spatial distribution of moment release may also indicate that the slip in the eastern portion of the fault plane is larger than in the western portion, although the resolution is poor.

DISCUSSION

The seismicity in global back arc regions has recently been very active. Large earthquakes with large tsunami occurred in a similar back arc region in the Japan Sea earthquake of 1983, the Costa Rica earthquake of 1991 and the Hokkaido-Nansei-Oki earthquake of 1993. It is interesting to note that these earthquakes are commonly modelled by composite faults at shallow depth [Aida, 1983; Imamura et al.,1993; Kikuchi,1993]. This point is very important because the heterogeneity and the depth extent of moment release are crucial to the excitation of a large tsunami. In each of the causes noted above, an island exists at the transition between two fault-segments, for example, Besar Island in this case, Kyuroku Island in case of the 1983 Japan sea event, and Okushiri Island in case of the 1993 Hokkaido-Nansei-Oki event. It seems likely that the rupture process might be influenced by the difference in geological structure near the island.

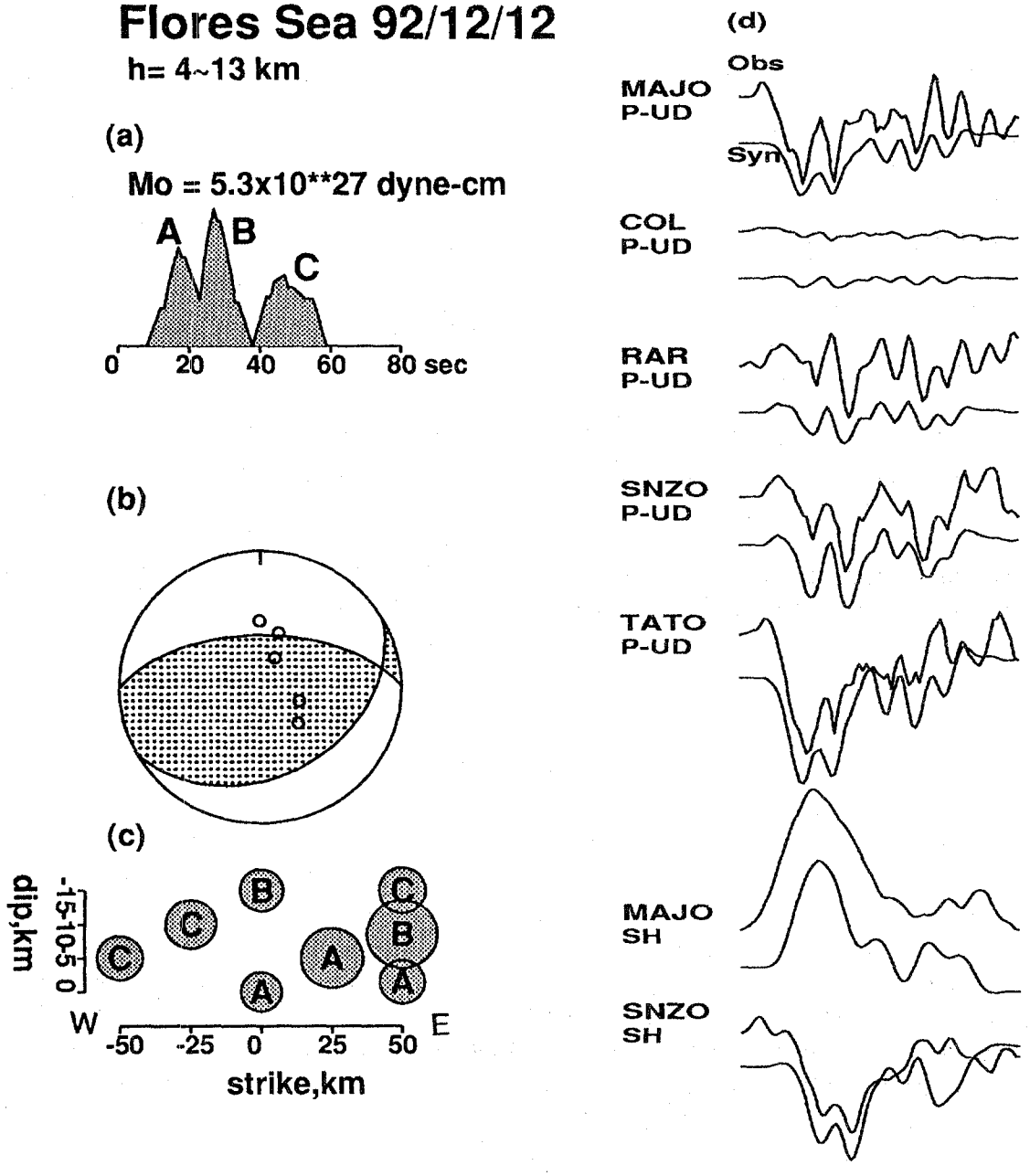

Figure 6: Result of teleseismic body wave inversion. (a) Source time function (b) Focal mechanism (c) Spatial distribution of the moment release on the fault plane (d) Comparison between observed (upper) and synthetic (lower) waveforms. The radius of the circles is proportional to the individual seismic moment. The symbol within the circles denotes the clusters corresponding to those in Fig.6(a).

CONCLUSIONS

A tsunami simulation in conjuction with teleseimic body wave inversion was used to investigate the moment release and depth extent of faulting of the 1992 Flores Island earthquake. The results show that the moment release was mainly shallow, and the slip in the eastern portion was larger than in the western portion. The event can be modelled by a composite fault with two fault segments which have different slip values: 3.2m and 9.6m. The fault mechanism is given as (strike,dip,slip) = (61°,32°,64°) and the depth of fault plane ranges from 3 to 15 km.

ACKNOWLEDGEMENTS

This study was partially supported by co-operative research grant from Ministry of Education, Science and Culture, Japan and the publication is financially supported by the Ogawa Commemoration Fund.

REFERENCES

Aida,I., Numerical source model of the 1983 Japan sea earthquake tsunami, *Bull. Earthq. Res. Inst. Univ. Tokyo*, 59, 93-104, 1984 (in Japanese).

Fitch,T., Plate convergence, transcurrent faults, and internal deformation adjacent to southeast Asia and the western Pacific,*J. Geophys. Res.*, 77, 4432-4460, 1972.

Gonzalez,F., S.Sutisna, P.Hadi, E.Bernard and P.Winnarso, Some observations related to the Flores island earthquake and tsunami,*Proc. Int. Tsunami Symp. in Wakayama*, 789-801,19 93.

Hamilton,W.B., Plate tectonics and island arcs, *Geological Soc.Am.Bull.*, 100, 1503-1527, 1 988.

Imamura,F., N.Shuto, S.Ide, Y.Yoshida and K.Abe, Estimate of the tsunami source of the 199 2 Nicaraguan earthquake from tsunami data,*Geophys. Res.Let.*, 20, 14, 1515-1518, 1993.

Imamura,F, T.Takahashi, S.Kawamata, M.Ortiz, T.Takahashi and N.Shuto, Study on the mechanism of the 1993 Hokkaido Nansei-oki earthquake from tsunami numerical analysis, *Progr. and Abst. of SSJ Meetin*g No.2 , A55, 1993 (in Japanese).

Kikuchi,M. and Y.Fukao, Iterative deconvolution of complex body waves from great earthquakes- the Tokachi-Oki earthquake of 1968, *Phys.Earth Planet.Inter.*, 37, 235-248, 19 85.

Kikuchi,M., Source process of the Hokkaido Nansei-Oki earthquake of July 12, 1993 inferred from teleseismic body wave inversion, *Progr. and Abst. of SSJ Meetin*g, No.2 , A28, 1993 (in Japanese).

McCaffrey,R., and J.Nabelek, The geometry of back arc thrusting along the eastern Sunda Arc, Indonesia - Constraints from earthquake and gravity data, *J. Geophys. Res.*,89, 6171-6179, 1984.

Silver,E.A., D.Reed and R.McCaffrey, Back arc thrusting in the easter Sunda arc, Indonesia: A consequence of arc-continent collision, *J. Geophys. Res.*, 88, 7429-7448, 1983.

Sunarjo, Experience in handling the Flores earthquake-tsunami of Dec. 12, 1992, *Proc. Int. Tsunami Symp. in Wakayama*, 861-869,1993.

Tsuji.Y., F.Imamura, Y.Kawata, H.Matsutomi, M.Takeo, M.Hakuno,J.Shibuya, M.Matsuyama and T.Takahashi, The 1992 Indonesia Flores earthquake tsunami, *Monthly Ocean*, 25 , 1-1 0, 1993. (in Japanese)

USGS, Flores region, Indonesia, *Seismologocal notes, BSSA*, 83,1632p., 1993.

Yeh,H., F.Imamura, C.Synolakis, Y.Tsuji, P.Liu and S.Shi, The Flores island tsunamis, *EOS, Trans. Am. Geophys. Union*, 74, 33,371-373, 1993.

A METHOD FOR REDUCING THE PROPAGATION NOISE IN FINITE-ELEMENT MODELING OF TSUNAMIS

Stefano Tinti, Ivan Gavagni

**Università di Bologna, Dipartimento di Fisica,
Settore di Geofisica, Viale Berti Pichat, 8
40127 Bologna, Italy.**

ABSTRACT

A Finite Element (FE) method to compute the propagation of tsunamis is presented in this paper. The numerical scheme includes a Smoothing Algorithm (SA) in the FE time-integration loop to prevent the numerical noise production and growth attributable to the dynamic tsunami propagation over the computational grid. The present SA is shown to be superior to the smoothing algorithm the authors have adopted in previous tsunami simulation studies. The main advantage of the new technique is that noise damping is obtained without practically affecting the total energy of the signal, that is of the tsunami, which makes it possible to calculate the tsunami evolution for a long time in the computational domain. The FE method illustrated here is applied to the nondispersive shallow-water approximation which is suitable for tsunami propagation modeling. The performance of the model is evaluated by comparing the numerical results with the analytical solutions that are available for rectangular uniform-depth basins in case of linear as well as nonlinear wave propagation.

INTRODUCTION

Numerical models of tsunami using the Finite-Element (FE) approach have been widely used since a long time, for they permit to adapt the computational grid to the irregular geometry of the basin domain, which is quite an important and advantageous property when tsunami propagation is to be studied in coastal areas characterized by complicated coastlines and/or bathymetry. FE models are known to be accurate when the grid element size is much smaller than the tsunami typical wavelength, but this condition cannot be always satisfied, since it often requires very fine meshes that are difficult to built and to handel. It is therefore important to device FE models that are capable to provide accurate results even on coarse grids. If we denote with ϵ the ratio between the characteristic element length and the dominant water wavelength, then we are able to formalize the distinction between coarse and fine grids: for our purposes, coarse grids correspond to ϵ values that are around 10^{-1}, while fine or very fine grids are associated with much smaller values of ϵ. Our interest in this paper will be devoted to studying FE models performance on coarse grids. In a previous investigation (Tinti and Gavagni, 1994) it was already shown that pure FE schemes are prone to noise production affecting the tsunami wave evolution, which can be counteracted by incorporating a smoothing algorithm in the basic FE time integration loop. Here we will present a further more efficient version of the noise damping algorithm, that is able to reduce the noise, meanwhile conserving the total energy of the signal. In the following we will speak of an "old" and of a "new" smoothing algorithm in order to distinguish between the first and the second version we have devised. The new algorithm is tested against analytical linear and nonlinear solutions in rectangular basins.

THE BASIC FE MODEL

The shallow-water approximation is known to be adequate to describe the tsunami propagation when the wavelength is much larger than the water depth, and will be adopted in this paper. If we designate with ζ, u and v respectively the water elevation above the mean sea level, and the horizontal velocity components, averaged over the water depth, the basic dynamic equations can be written as:

$$\begin{cases} \partial_t \zeta = -\partial_x (Du) - \partial_y (Dv) \\ \partial_t u = -g\partial_x \zeta - u\partial_x u - v\partial_y u \\ \partial_t v = -g\partial_y \zeta - u\partial_x v - v\partial_y v \end{cases} \tag{1}$$

Here h is the water depth, g is the gravity acceleration and $D = h+\zeta$ is the instantaneous water depth. The dynamic fields are computed in a finite domain that is enclosed within a boundary on which they have to satisfy suitable conditions. Imposing that the wave be totally reflected on the coasts and be completely transmitted through the open sea boundaries implies that:

$$\vec{v} \cdot \vec{n} = 2(c_1 - c_0) \quad \text{on the open boundary} \tag{2a}$$

$$\vec{v} \cdot \vec{n} = 0 \quad \text{on the solid boundary} \tag{2b}$$

Here $\vec{v}$ is the horizontal velocity vector, while $\vec{n}$ is a unit vector normal to the boundary and oriented outward. Furthermore $c_1 = \sqrt{g(h+\zeta)}$ represents the local phase velocity and $c_0 = \sqrt{gh}$ is the phase velocity of the linear wave. It may be easily shown that when ζ is much smaller than h, the expression (2a) reduces to:

$$\vec{v} \cdot \vec{n} = \frac{g}{c_0}\zeta \quad \text{on the open boundary} \tag{2c}$$

which is suitable for the linear approximation. After covering the space domain with a N-node grid, the above system of equations (1) can be discretized in space by means of the Galerkin procedure (see Tinti, Gavagni and Piatanesi, 1994 for details), which leads to a set of ordinary differential equations of the form:

$$A\dot{\widetilde{\xi}}(t) = B(\widetilde{\xi})\widetilde{\xi}(t) \tag{3}$$

for the $3N$-component vector $\widetilde{\xi}$ representing the nodal values of the dynamic fields ζ, u and v. In these equations the matrix of stiffness A is formed by 3 N by N diagonal blocks K and is constant in time:

$$A = \begin{pmatrix} K & 0 & 0 \\ 0 & K & 0 \\ 0 & 0 & K \end{pmatrix} \tag{4}$$

while the operator B changes dynamically since it depends on the unknown vector $\widetilde{\xi}$ itself. The above equation (3) can be discretized in time, by means of a solving scheme that is accurate up to the second order in the integration time step Δt and that provides solutions fullfilling the boundary conditions (2) (see Tinti and Gavagni, 1994):

$$\begin{cases} \widetilde{\chi}_{n+\frac{1}{2}} = \widetilde{\xi}_n + \frac{1}{2}\Delta t A^{-1} B(\widetilde{\xi}_n)\widetilde{\xi}_n \\ \widetilde{\xi}_{n+\frac{1}{2}} = C\widetilde{\chi}_{n+\frac{1}{2}} \\ \widetilde{\chi}_{n+1} = \widetilde{\xi}_n + \Delta t A^{-1} B(\widetilde{\xi}_{n+\frac{1}{2}})\widetilde{\xi}_{n+\frac{1}{2}} \\ \widetilde{\xi}_{n+1} = C\widetilde{\chi}_{n+1} \end{cases} \tag{5}$$

Here it has been implicitly defined that $\widetilde{\xi}_n$ is the value that the vector assumes after n integration loops, that is $\widetilde{\xi}_n = \widetilde{\xi}(t_0 + n\Delta t)$. Furthermore, it has been introduced the operator C which has the property of transforming the auxiliary intermediate vector $\widetilde{\chi}_n$ in a vector $\widetilde{\xi}_n$ satisfying the boundary conditions. Starting from a specified initial condition $\widetilde{\xi}_0 = \widetilde{\xi}(t_0)$, the scheme (5) is applied repeatedly until the final time $T = t_0 + N_{tot}\Delta t$ desired for the tsunami simulation is reached, N_{tot} being the total number of time iterations. It is useful to observe that the 4 steps in the loop (5) can be distinguished in two dynamical steps, the first and the third, deriving from the discretization of the shallow-water equations (1), and in two static steps, the second and the fourth, that correspond to the boundary conditions (2). Fine-grid stability criteria suggest that

the time integration step Δt must be taken smaller than the smallest grid-element crossing time ΔT to perform computations. We emphasize that, when coarse FE grids are handled, respecting this condition is insufficient to prevent numerical noise growth, which instead must be controlled by means of specific algorithms.

THE SMOOTHED FE MODEL

By a Smoothed FE (SFE) model it is meant here a model where the basic integration cycle (5) is modified in order to introduce computational smoothing processes capable of reducing the numerical noise. We observe that noise is produced by the two dynamical steps of the integration loop (5), that compute the free propagation of the wave over the grid, as well as by the two static steps accounting for the wave-boundary interaction. In this paper we address our interest mostly to controlling the first kind of noise. From a formal point of view the 4-step loop (5) can be synthetically reproposed by means of a nonlinear operator L:

$$\widetilde{\xi}_{n+1} = L(\Delta t, \widetilde{\xi}_n)\widetilde{\xi}_n \tag{6}$$

that depends on the time step Δt as well as on the field itself $\widetilde{\xi}_n$ and that transforms the solution computed at the time t_n into that one at the time $t_n + \Delta t$. Let us suppose that L generates numerical noise, which implies that, even if $\widetilde{\xi}_n$ were unaffected, $\widetilde{\xi}_{n+1}$ is corrupted by noise and can be decomposed into:

$$\widetilde{\xi} = \widetilde{s} + \widetilde{n} \tag{7}$$

where $\widetilde{s}$ is the signal vector, $\widetilde{n}$ is the perturbing noise vector, and the subindex $n+1$ is dropped for clarity. Our purpose now is to estimate the signal $\widetilde{s}$ from the computed total vector $\widetilde{\xi}$. Bearing in mind that $\widetilde{\xi}$ represents the three physical fields ζ, u and v, it results more convenient to apply the estimation procedure separately on each individual field. If we call E_f the single field estimator, the total estimate operator E can be given the following block-diagonal form:

$$E = \begin{pmatrix} E_f(\widetilde{\zeta}) & 0 & 0 \\ 0 & E_f(\widetilde{u}) & 0 \\ 0 & 0 & E_f(\widetilde{v}) \end{pmatrix} \tag{8}$$

where it is explicitly emphasized the E_f acts on the N-component fields $\widetilde{\zeta}$, $\widetilde{u}$ and $\widetilde{v}$ in a non linear way. We observe that E does not necessarily give rise to vectors satisfying the boundary conditions, but if we combine E with the operator C, we obtain an estimator, say $E_C = CE$ respecting the constraints, and consequently we can state that:

$$\widetilde{s} \simeq E_C(\widetilde{\xi})\widetilde{\xi} \tag{9}$$

In other words E_C is an operator that is capable of separating the signal from the noise and that can be used repeatedly during tsunami simulation experiments. From

the foregoing, it is easy to envisage that the core loop of a SFE model can be simply written as:

$$\widetilde{\xi}_{n+1} = E_C(\widetilde{\xi}_n)L(\Delta t, \widetilde{\xi}_n)\widetilde{\xi}_n \tag{10}$$

In practical applications, however, since the noise production is generally quite slow, it is not necessary to make use of the SFE loop at any integration time step Δt, but only at time steps Δt_S that are multiples of Δt, i.e $\Delta t_S = k\Delta t$. Therefore an SFE model consists in intercalating the integration SFE cycle (10) regularly in the sequence of the FE loops (6), the frequence of the application of (10) depending on the efficiency of the noise production.

Let us now concentrate on the field estimator E_f on which the whole estimation process is founded. In a previous paper (Tinti and Gavagni, 1994) a field estimator process was introduced that was based on a Least Squares (LS) approximation: given a node i, the field in the neighbourhood of the node is approximated by means of a polynomial surface whose parameters are determined by LS best fitting. The value the approximating surface assumes at the node is taken as the estimator of the field, and the process is iterated for all the nodes of the computational grid. Cubic polynomials involving as many as 10 parameters were shown to be sufficient to provide a satisfactory reduction of the numerical noise combined with an acceptable computational extracost. In this paper we will illustrate a new estimation process that is an improved variant of the prior procedure and that is able to calculate better wave solutions especially in the long run. The main disadvantage of the LS best fitting is that, though it is indeed very effective in lowering the noise, yet at the same time it affects slightly even the main signal. The effect is often unimportant, especially if the interest is focussed on the near-field short-range tsunami propagation, but it becomes progressively more relevant as time passes owing to the repeated application of the SFE loop, and at the end it may determine a sensible abatement of the wave energy. The basic explanation lies in the fact that LS estimates produce smoothed waveforms, tending to flattening crests and troughs and to broadening the wavebase, as can be appreciated in the examples that will be shown later on. The new field-estimator algorithm has been devised with the purpose of conserving the good property of the LS approximation as regards noise lessening and of correcting its tendency to rounding off local waveform extremes. In the following of the paper the two methods will be designated by "old" and "new" Smoothing Algorithms (SA). Formally the field estimator can be given the expression:

$$\widetilde{g} = E_f(\widetilde{f})\widetilde{f} \tag{11}$$

where $\widetilde{f}$ represents any of the N-component field vectors $\widetilde{\zeta}$, $\widetilde{u}$, or $\widetilde{v}$, whereas $\widetilde{g}$ is the noisefree estimate of the field. Let us now admit that the estimator E_f in the formula (11) be the old LS estimator. The new estimator does not act on the original field $\widetilde{f}$, but instead on a conveniently manipulated field that is obtained by first scaling $\widetilde{f}$ through an operator S_f and then by transforming the resulting field through a further operator T_f. If we introduce the operator D_f defined by $D_f = T_f S_f$, in place of the above equation (11) we will use the expression:

$$\widetilde{g} = D_f^{-1} E_f(D_f\widetilde{f})D_f\widetilde{f} \tag{12}$$

that constitutes the basis of the new version of the Smoothing Algorithm. Scaling is performed simply by dividing each field component f_i by a scaling factor f_M, where $f_M = \max \mid f_i \mid \quad i = 1,2,\ldots,N$. After introducing the scaled field $\widetilde{f}^S$, the above scaling law may be expressed by:

$$f_i^S = f_i / f_M \quad i = 1,2,\ldots,N \tag{13}$$

The subsequent transformation consists in an amplification of the local extremes of the field, which is conceived in such a way to counteract the flattening resulting from the LS estimator. Many preamplification algorithms have been tested. That experimented here is convenient because it is quite a simple one-parameter function. It is given by:

$$f_i^T = \text{sign}(f_i^S) \mid f_i^S \mid^{\frac{1}{p}} \quad i = 1,2,\ldots,N \tag{14}$$

where the parameter p has to be suitably selected. Here f_i^T denotes the i-th component of the preamplified field $\widetilde{f}^T$, that will be subsequently used as the input of the LS estimator E_f, according to the expression (12). We observe that if p is chosen equal to 1, the law (14) reduces to the identity, whereas for $p > 1$, it acts as a proper amplification law, since $f_i^T > f_i^S$. On the contrary, when $0 < p < 1$, it results $f_i^T < f_i^S$ and the law does not suite our purposes. We remark moreover that the amplification (14) is applied only in the neighbourhood of the local extremes, that is in proximity of the local minima and maxima of the wave field. Far from these regions, the basic LS estimator (11) is found to perform quite well and does not require any additional sophisticated corrections. In the following section, the new SA (12) will be tested against the old SA (11) as well as against the pure FE model with no smoothing incorporated. The analysis of the results will help us appreciate the enhanced performance of the new version of the SA.

NUMERICAL EXPERIMENTS

Numerical tests have been carried out for simple 1D cases admitting analytical solutions, since they provide us good reference fields for the evaluation of the numerical results. In the first set of experiments we consider the linear propagation of a dipole wave, with a leading depression followed by a crest, in a flat-bottom rectangular basin that is closed by vertical reflecting walls. The basin is covered either by a regular grid of equal-size triangles or by a second grid which is densified at the left and right basin ends, as is respectively shown in the upper and lower panel of the Figure 1. The initial wave is laterally uniform which implies a 1D theoretical evolution along the basin longitudinal axis. The wave possesses initial potential and kinetic energy and theoretically travels unchanged towards the left end of the basin. Here it is back reflected and then propagates towards the right end, where it experiences a further reflection which forces it to travel leftward, until it reaches again its initial position. The propagation proceeds periodically, with the wave travelling at constant velocity back and forth along the channel with no energy loss. The wavelength is only a few grid untis, which makes it a case belonging to the category of waves travelling on a coarse grid, as we want to tackle here.

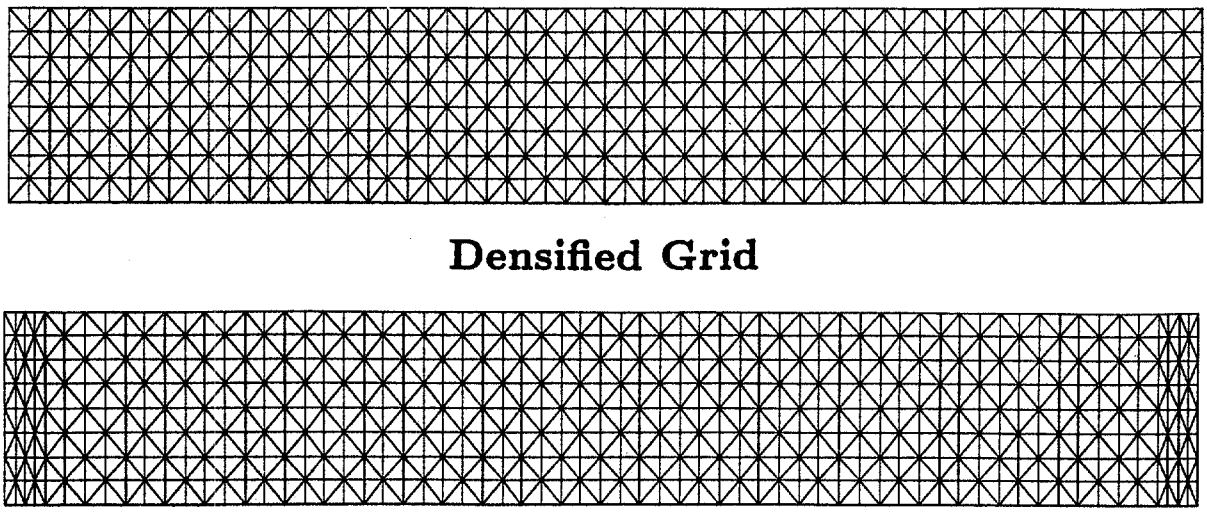

Figure 1. *Rectangular grids used in the numerical experiments.*

The solution is calculated first over the Regular Grid (RG) by means of the pure FE model that involves the loop (5), using the time step $\Delta t = 5$s. Elevation profiles along the central axis of the basin are displayed in Figure 2 every 150s together with the theoretical solution. It may be seen the dipole approaching the left basin wall (upper panel), the wave interacting with the wall (central panel) and the wave travelling rightward after reflection has taken place (lower panel). This short-interval propagation experiment shows that the numerical wave is close to the theoretical solution, but it is alterated by noise that tend to increase with time: this is evident in the post-reflection stage where the wave height is often smaller than the expected signal and where a background disturbance in the dipole front and tail has already reached a remarkable level. The same case has been then solved by means of the old SA, based on the integration cycle (10). The smoothing time step Δt_S has been taken equal to 20s, that is four times larger than the integration time step Δt. Figure 3 shows the computed wave profiles, that serve us to evidentiate the good features of the algorithm as well as its weakness points. At the first glance, the waveforms appear to be more regular and "clean". The short-wavelength noise disturbances have been properly treated by the old SA and consequently cannot be seen even after 3000 seconds corresponding to as many as 600 time integration cycles. As the effect of its application, however, the wave shape is changed, since the signal is both smaller and broader in the final stages. The third numerical experiment concerns the new SA, which is applied on the same grid and with the same time step values, namely $\Delta t_S = 20\text{s} = 4\Delta t$, to allow a fair comparison with the other cases. The results are plotted in Figure 4 and have been obtained with the value of the parameter p in the amplification law (14) equal to 2.5. Looking at the graphs, it can be appreciated that 1) the noise has been practically removed; 2) the wave broadening is much smaller than that for the old SA; 3) the wave maxima and minima are better reproduced. The comparison of the solutions can be completed by analysing the energy graphs that are displayed in Figure 5. The potential, kinetic as well as the total energy in the whole basin are computed for the theoretical case and for all the numerical simulations. We point out that what we call here theoretical energy does not exactly coincide with the correct solution, since our computations take into

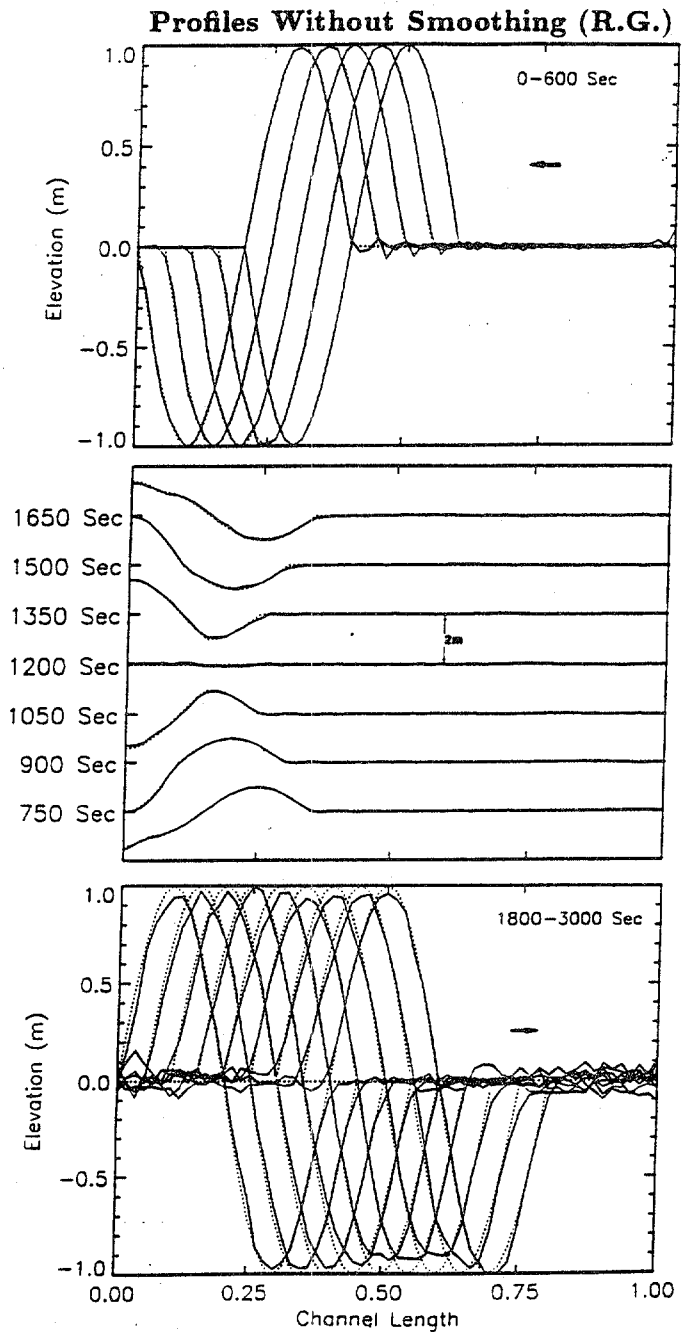

Figure 2.
Wave profiles computed for the dipole propagation in the Regular Grid shown separately prior to, during and after the wave interaction with the wall. Computations are made through the pure FE model and are compared with the analytical solution.

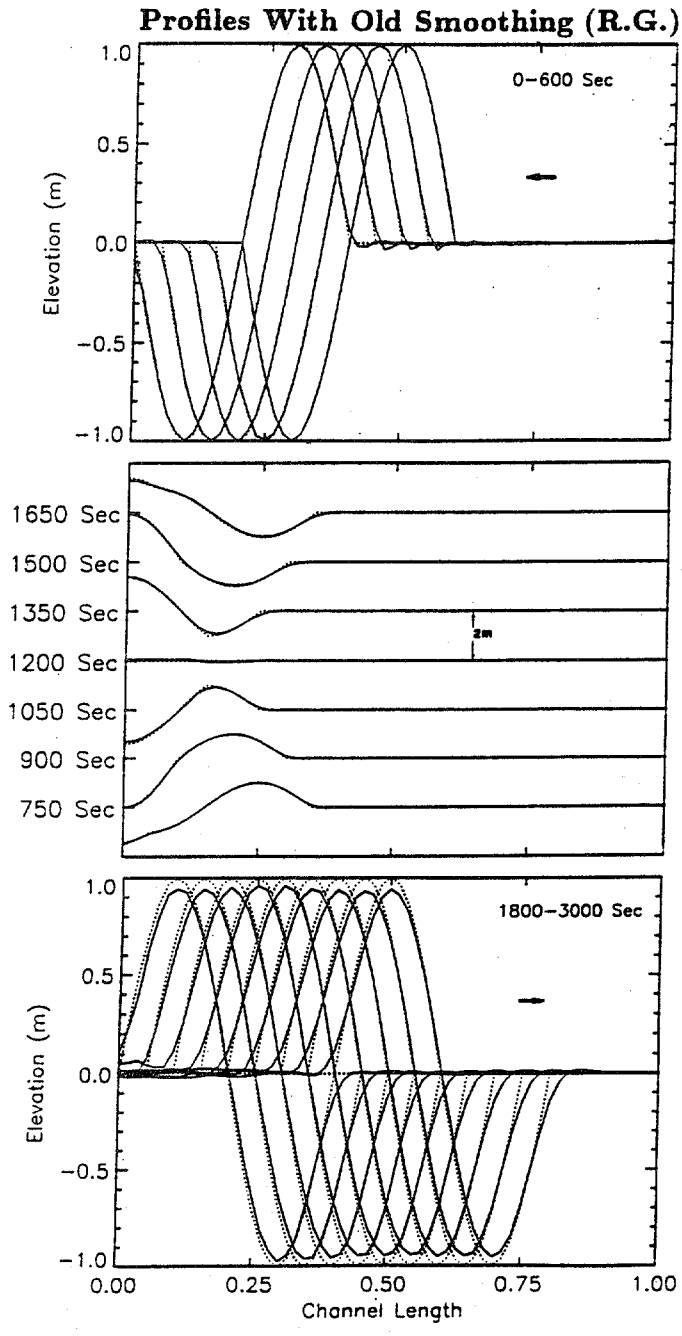

Figure 3.
Wave profiles calculated via the old SA scheme.

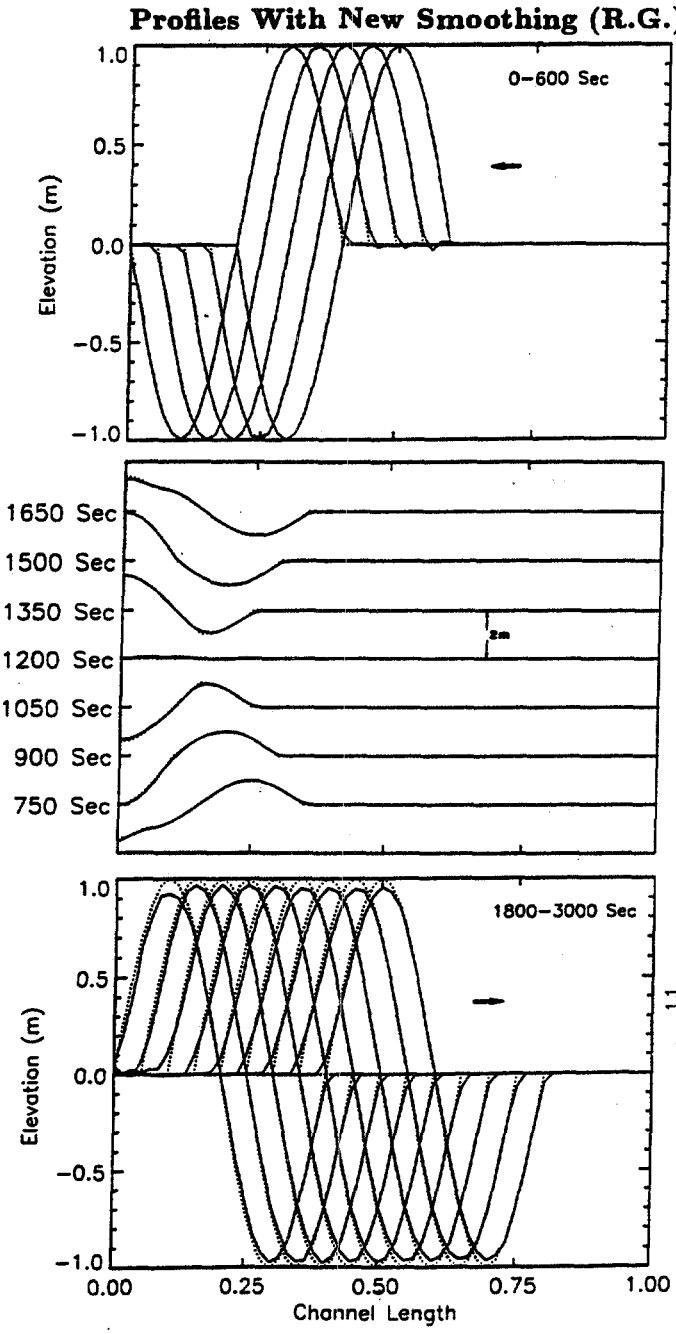

Figure 4.
Wave profiles computed by means of the new SA scheme.

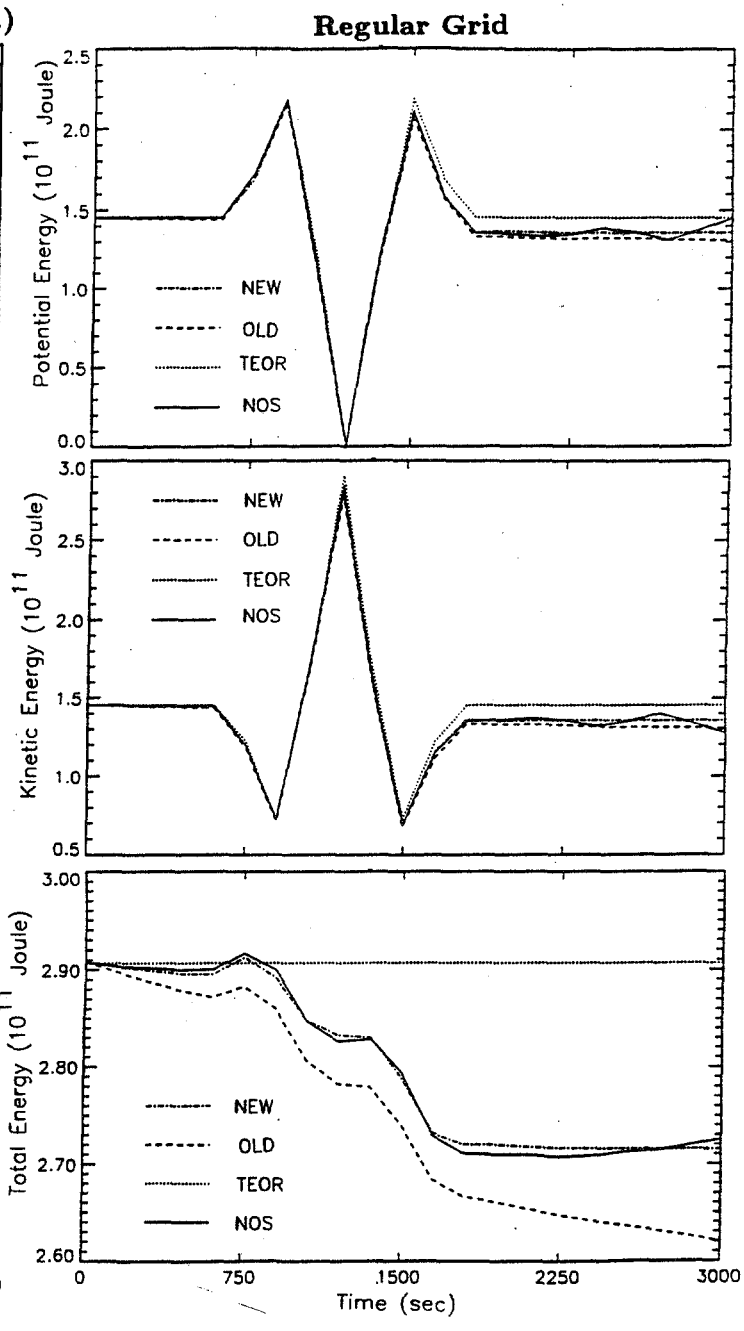

Figure 5.
Plots of the wave energy in the whole basin computed with all the methods: pure FE, old SA and new SA.

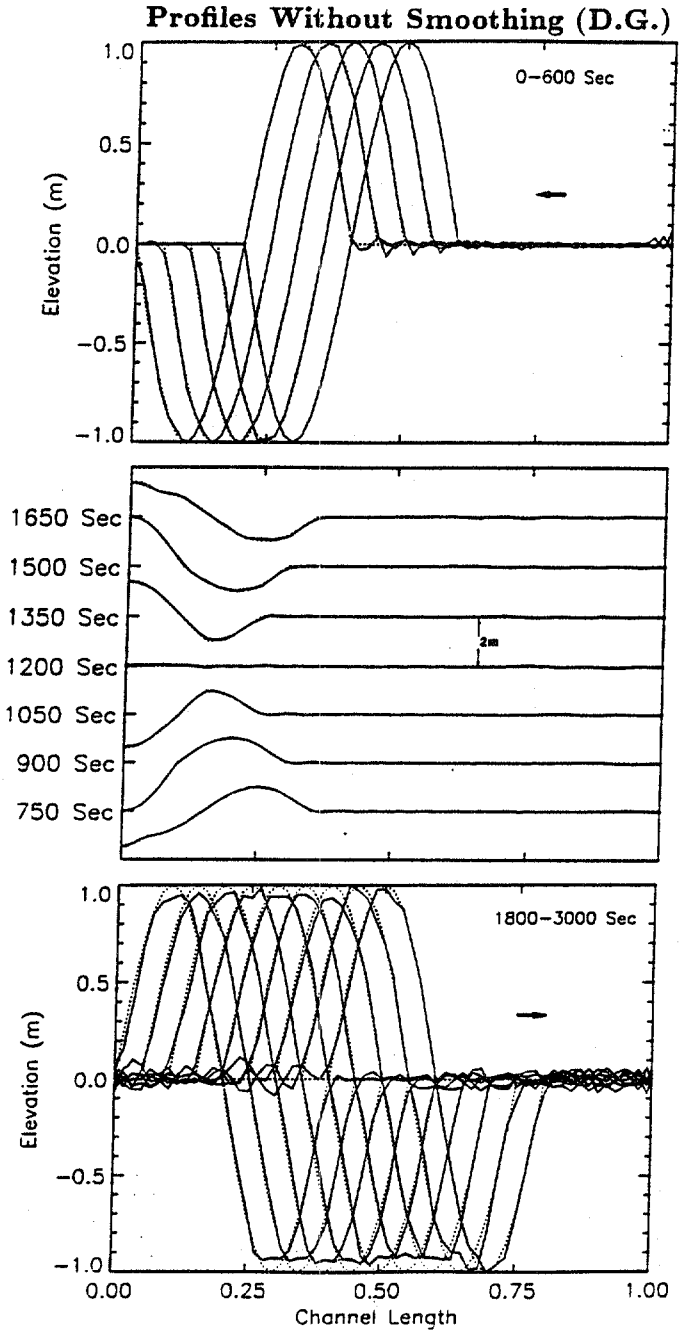

Figure 6.
Wave profiles computed in the Densified Grid through the basic FE model.

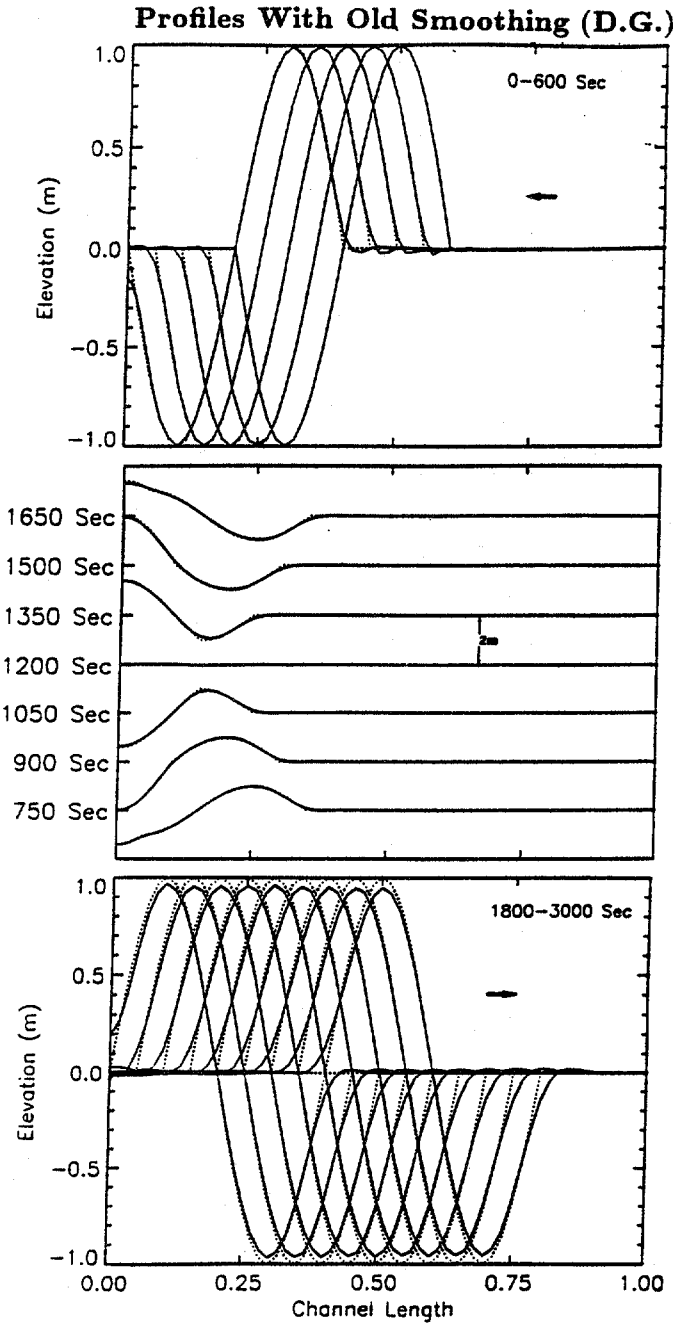

Figure 7.
Wave profiles resulting from the old SA model.

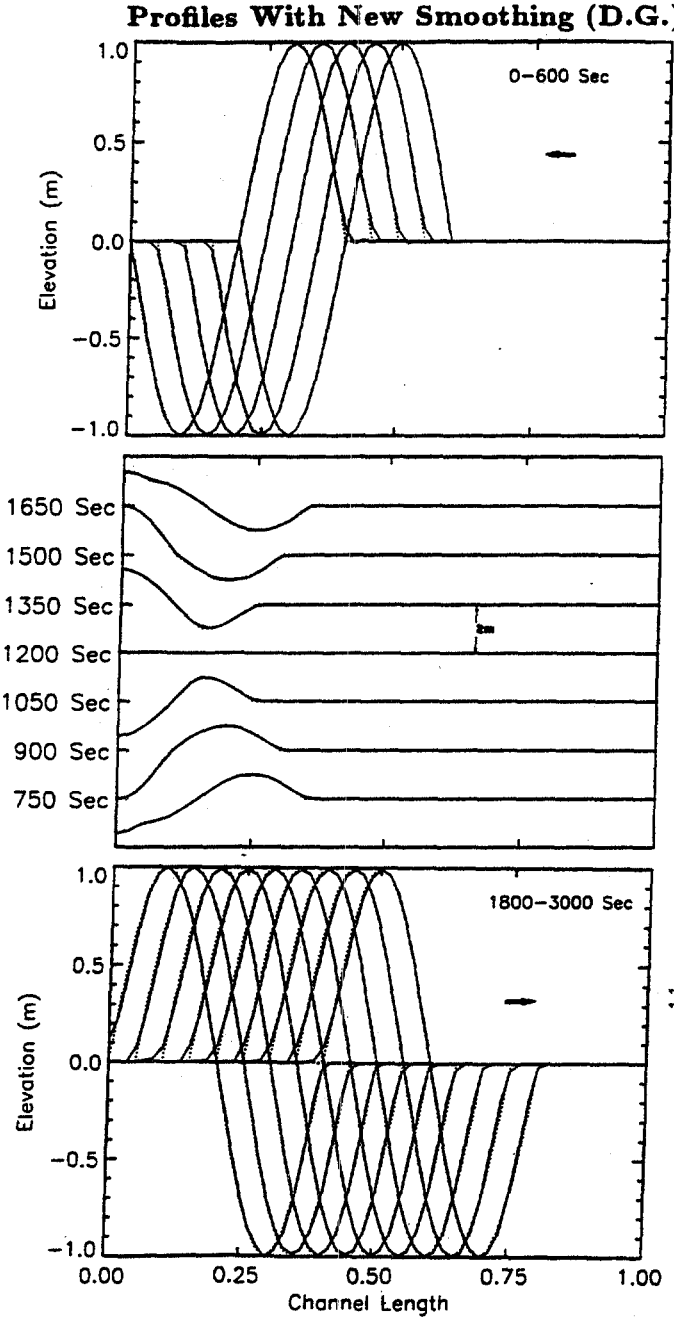

Figure 8.
Wave profiles calculated through the new SA model.

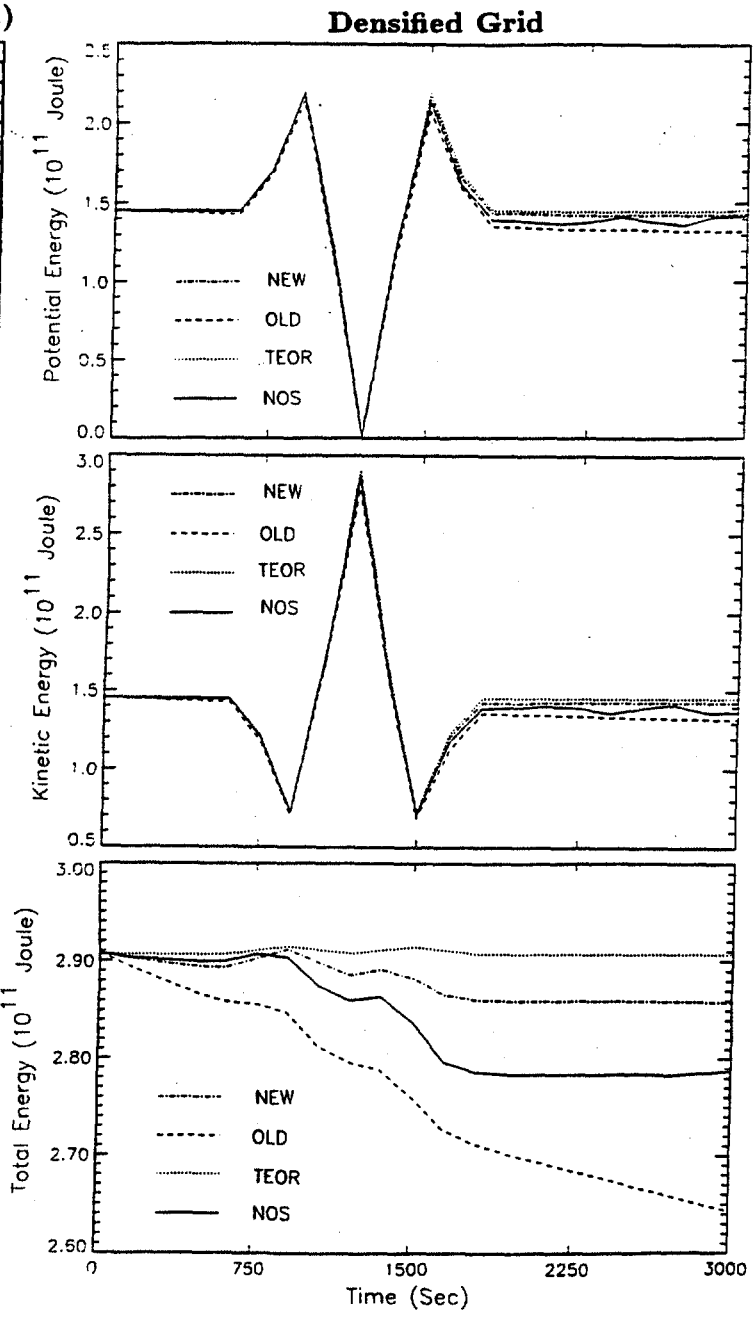

Figure 9.
Plots of the wave energy in the whole basin computed with all the methods: pure FE, old SA and new SA.

account the grid discretization: the energy in the channel is indeed calculated i) by taking the analytical field values at the mesh nodes which are correct and then ii) by integrating over the grid under the assumption of a linear interpolation function, which is incorrect, though consistent with the Galerkin discretization process that is at the basis of our FE model. This latter step necessarily introduces some discrepancy with the analytical energy, but, given a certain grid, this discrepancy cannot be eliminated. The theoretical values represent therefore the best possible solution that can be obtained by any numerical methods over the chosen grid and can be accordingly taken as useful reference values. What can be learned from Figure 5 is that all numerical energy plots exhibit a loss of energy, which is quasi equipartitioned between the potential and the kinetic part. The rate of energy loss is much larger during the wave-boundary interaction phase, taking place from 600-1650s. The old SA solution has approximately the same energy loss rate before and after the wave reflection. The new SA solution shows a smaller energy decrease, which is however almost totally attributable to the reflection case. The pure FE solution has an energy graph that is surprisingly similar to the new SA plot, which could suggest that our new SA leads to no sensible improvement over the basic FE scheme: this is however misleading. Infact, if we come back to the wave profiles, we can observe that practically all energy of the SA wave derives from the signal, whilst the energy of the pure FE solution is contributed both by the signal tending to diminish and by the noise tending to get larger. Eventually the noise growth exceeds the signal degrade rate and is responsible of the total energy increase that is visible at the final times of the pure FE energy graph. The main conclusion that can be drawn is that the new SA is able to kill the noise and to conserve appreciably the wave energy during the free propagation phase where no interaction with the boundary is taking place.

As regards the reflection at the boundary, a simple way to improve the solution is to use a locally refined grid. We have used the mesh that is shown in the lower panel of Figure 1 and that we identified as the Densified Grid (DG). The experiments carried out with the basic FE method, the old SA and the new SA lead to the wave profiles that are given in the order in Figures 6-8. The same comments that have been made for the previous cases can be repeated also here, having however in mind that the solutions are now globally more satisfactory. In particular we call the attention on Figure 8 showing that the curves computed through our new method approximate the theoretical profiles extraordinarily well. The energy plots (see Figure 9) confirm that the new SA solution is largely superior to the other numerical results. The loss of total energy at the end of the 3000s computational interval is as small as $\sim 1.7\%$ and is to be compared with the 4.0% loss produced by the pure FE case (signal+noise) and with the over 9.5% loss associated with the old SA field (only signal). In order to evaluate the performance of the SA scheme we have also performed long-run experiments, where the wave propagation back and forth in the channel has been computed for as many as three full wave cycles, namely for 18000s. Periodic propagation implies that after a cycle is completed, the wave assumes exactly the same position and velocity it had at the beginning of the cycle. This property may be used to judge the wave propagation model. The discrepancy of the numerical wave from its initial shape provides a measure of the model performance.

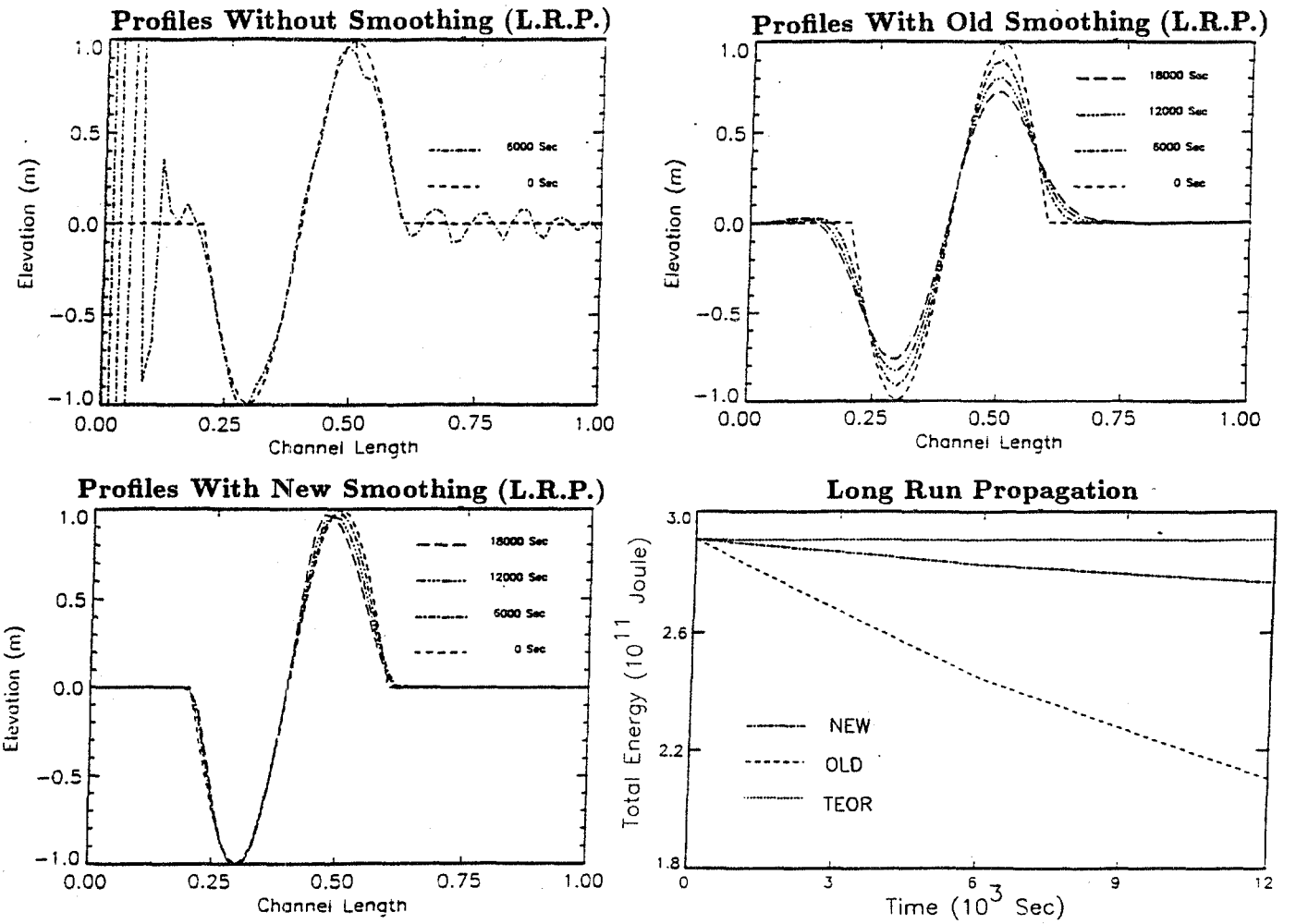

Figure 10. *Long-run propagation of the wave dipole over the Densified Grid. Computed wave profiles at the end of the first three cycles as well as plots of the total energy in the basin vs time.*

Figure 10 gives us wave profiles computed as usual through the basic FE as well as via the old and the new SAs at the end of the first, the second and the third cycle. The Figure also shows the plot of the total wave energy vs time for all cases. When no smoothing is applied, the dipole evolution cannot be computed beyond the first period, since the numerical noise degrades the solution to such a degree to become dominant and to explode. This is a demonstration that pure FE models do not perform well for the long-run propagation on a coarse grid and need to be modified. The old SA calculates waves that are free from noise instabilities. The position of the wave at the end of each period is correct, but waves become smaller and wider loosing progressively energy, the final field possessing about the 70% of the energy initially available. The new SA exhibits the best performance, since it computes both the wave position and height in a satisfactory wave, though some small distorsion of the wave shape is visible

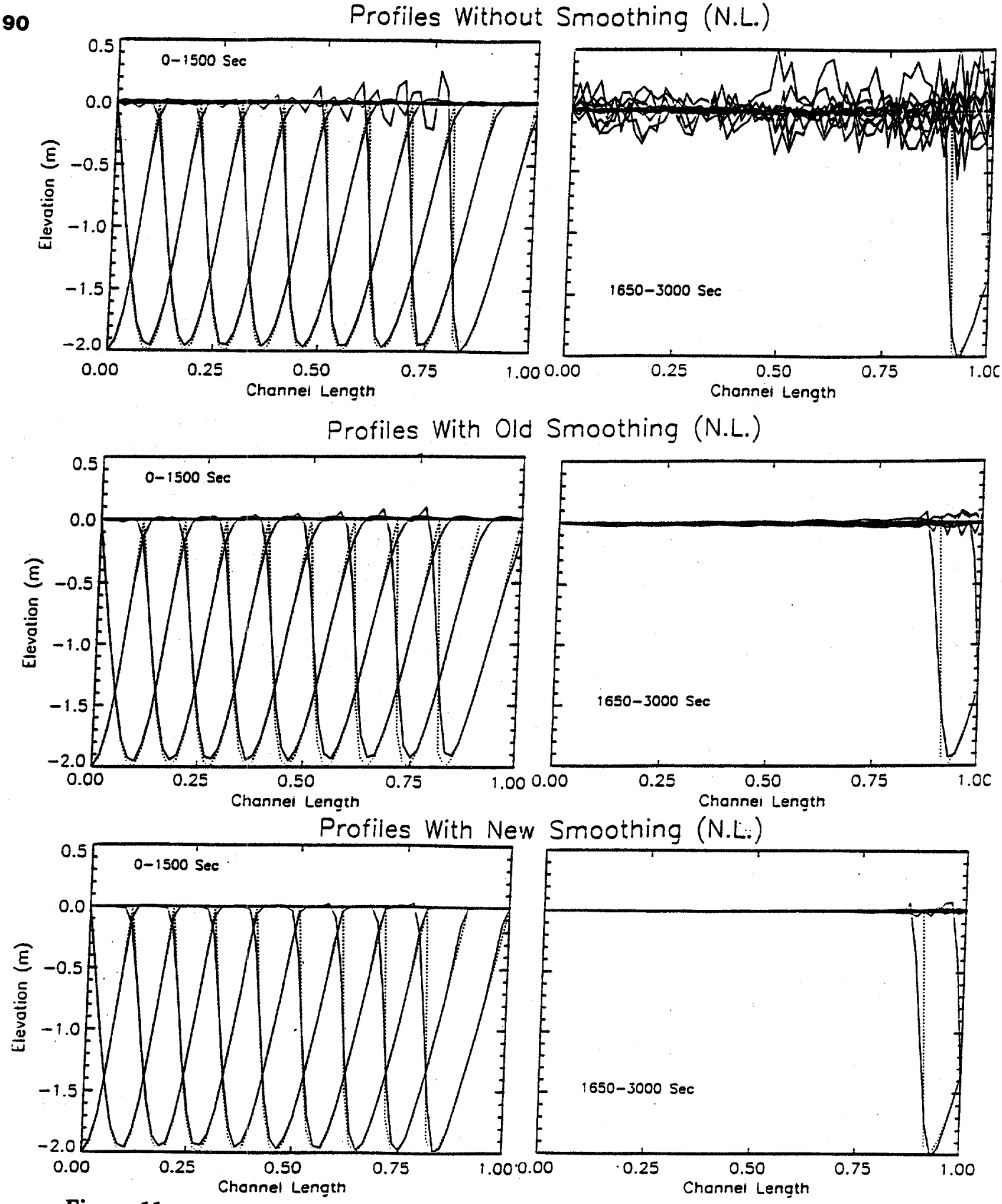

Figure 11.

Nonlinear propagation of a depression in an open channel covered by the Regular Grid. The wave propagates rightward, leaving eventually the basin. Results corresponding to the pure FE, old SA and new SA are plotted.

from the Figure. In this case the energy loss amounts to only 5% of the initial energy and is mostly attributable to the wave reflection against the boundaries rather than to the wave propagation in the channel.

The last case we present here regards the nonlinear propagation of a disturbance in the channel. The purpose is to show that the algorithm we have devised functions properly even for the fully nonlinear shallow water equations given in (1). The basin is a channel open at both left and right ends, which is covered by the regular grid shown in Figure 1. The wave is a water depression that is assumed to enter the channel from the left, which numerically implies that the nodes on the left boundary are forced to move according to a prescribed time law. The wave propagates rightward until it leaves the channel through its left end. The numerical simulations compute the wave evolution during a time interval of 3000s which is sufficient to cover the complete wave passage across the channel until the water resumes its initial still condition. What we can observe in Figure 11 is concordant with the results of the previous experiments. The basic FE model calculates noisy solutions: specifically the depression travels with a disturbance growing on its tail, which cannot leave the basin and that, after the wave passage, adds to the residual background noise. The old SA reduces the noise and mildly the signal, leaving however some residual perturbation in the channel, while the new SA computes a "clean" travelling wave that crosses the left end with practically no energy left inside the channel. This may be also seen in the energy plot curves given in Figure 12.

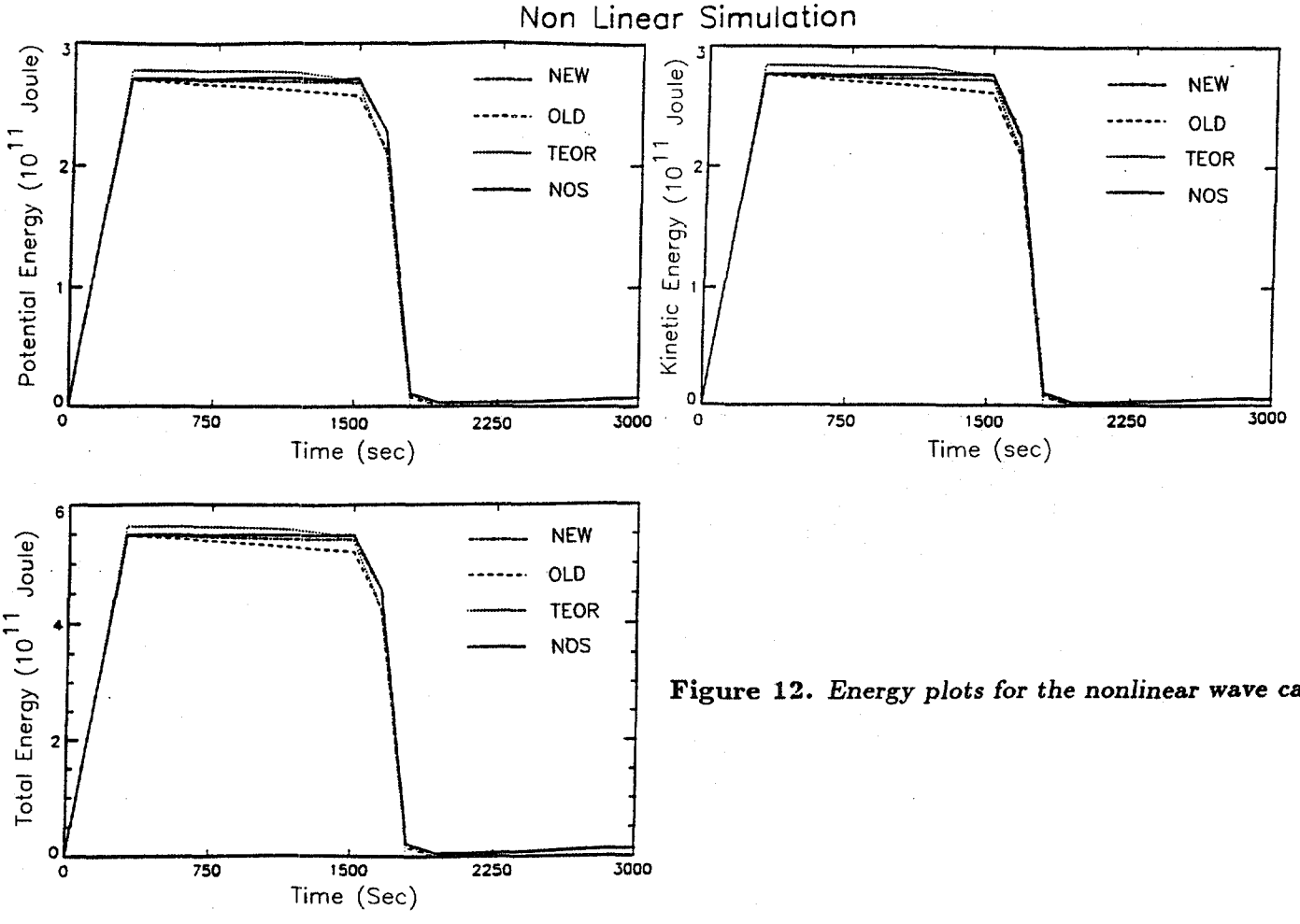

Figure 12. *Energy plots for the nonlinear wave case.*

CONCLUSIONS

In this paper we have elucidated the limits of the finite-element integration scheme for long water wave propagation over a coarse grid. We have shown that the model computations are affected by numerical noise which is produced constantly and eventually makes the results meaningless: this implies that the FE model is reliable only in the very short-run. This calls for the implementation of proper corrective algorithms suitable to controlling the noise generation. Two versions of smoothing algorithms have been discussed here: the former illustrated in a previous paper eliminates the noise, affecting however the signal as well, with unsatisfactory results in the long-run. The latter, that has been called the new SA, has the double advantage of eliminating the propagation noise and to treat properly the signal even for long intervals of time. The efficiency of the algorithms has been shown only for 1D cases, but the model is conceived to be applied to complicated grids and for arbitrary initial conditions. We remark that this study does not exhaust the problem and that further research is needed to device better algorithms. The long-run experiment has shown that the new SA does cause a small distorsion of the wave, that further investigations should try to avoid. And most importantly, a nonnegligible source of noise that has not been dealt with here may be identified in the boundary conditions, both for the closed reflecting walls as well as for the open transmitting boundaries.

ACKNOWLEDGMENTS

This research was supported partly by the "Consiglio Nazionale delle Ricerche" (CNR) and partly by the "Ministero dell' Università e della Ricerca Scientifica e Tecnologica" (MURST). This research made use also of specific European Union funds (Contract EVCV-CT92-0175).

REFERENCES

TINTI S. and GAVAGNI I., 1994. A smoothing algorithm to enhance Finite-Element modeling: an application to the 5 February 1783 Calabrian case, Italy, Natural Hazards, (submitted).

TINTI S., GAVAGNI I. and PIATANESI A., 1994. A finite-element numerical approach for modeling tsunamis, *Annali di Geofisica*, **37**, 1009–1026.

MANIFESTATION OF HOKKAIDO SOUTHWEST (OKUSHIRI) TSUNAMI, 12 JULY, 1993, AT THE COAST OF KOREA: 1. STATISTICAL CHARACTERISTICS, SPECTRAL ANALYSIS, AND ENERGY DECAY

Im Sang OH

Department of Oceanography, College of Natural Sciences,
Seoul National University, Seoul
151742 KOREA

Alexander B. RABINOVICH

Institute of Marine Geology and Geophysics,
Russian Academy of Sciences, Yuzhno-Sakhalinsk,
693002 RUSSIA

ABSTRACT

A strong earthquake with magnitude M = 7.8, which occurred on 12 July, 1993 in the northwestern part of the Sea of Japan, caused a catastrophic tsunami. This tsunami was clearly manifested on the coast of the Republic of Korea and was recorded by 6 tide gauges. The records are examined by means of statistical and spectral analysis.

Evident differences in observed characteristics of tsunami waves at various stations (wave heights, periods, duration of tsunami oscillations, energy decay, etc.) demonstrate a strong influence of local topography. The highest waves were observed on the northeastern coast in the region of the Mukho station where trough-to-crest heights were up to 2.72 m. In comparison with an open sea island station, Ulleungdo, tsunami waves on this coast (at the stations Mukho and Sokcho) amplified 2-3 times. On the contrary, tsunamis on the southeastern coast (Pohang, Ulsan, Pusan) were 1.5-4 times weaker than in Ulleungdo.

The decay of local tsunami energy was estimated. The corresponding decay times T_0 (in hours) were found to be: 3.1 (Ulleungdo), 3.9 (Sokcho), 5.7 (Mukho), 8.5 (Pusan) and 13.3 (Pohang). Significant differences in these values prove that they are related to the Q-factors of the corresponding local domains rather than to the Q-factor of the Sea of Japan as a whole or to the peculiarities of the source area.

Comparative spectral analysis of the data showed that the principal tsunami energy concentrated at comparatively high frequencies, peaking at 0.12 cpm (period 8.5 min). This means that the initial tsunami source area was relatively small. The essential topographical amplification of tsunami waves approaching the coast of Korea took place at the frequencies below 0.15 cpm.

1. INTRODUCTION

A strong earthquake occurred on 12 July, 1993 at 22:17 Korean Time (13:17 GMT) in the northeastern part of the Sea of Japan (East Sea) off the southwestern coast of Hokkaido Island, Japan. The parameters of the earthquake according to different sources were as follows:

Japan Meteorological Agency (JMA):
Latitude = 42.78° N; Longitude = 139.18° E; Depth = 35 km;
Ms = 7.8; Seismic intensity I = 6; Tsunami intensity m = 3.

Harvard, USA:
Latitude = 42.63° N; Longitude = 139.24° E; Depth = 15 km;
Mw = 7.8; Duration = 16.6 sec.

Geological Survey, USA:
Latitude = 42.842° N; Longitude = 139.289° E; Depth = 17 km;
Mw = 7.3; Ms = 7.6 (GS); Ms = 7.4 (BRK).

Obninsk, Russia:
Latitude = 42.83° N; Longitude = 139.21° E; Depth = 40 km;
Ms = 8.0.

The epicenter of the earthquake was located near a small Japanese island Okushiri (Fig.1). Source characteristics were estimated by Harvard University scientists based on magnitude Mw and aftershock data. They assumed fault width and length of 50 km and 150 km respectively, shear modulus of $3*10^{11}$ dyne/cm^2 and an average slip of 2.5 m on the fault plane. The focal mechanism has one modal plane dipping directed eastward at 24° from the horizontal (*Bernard et al.*, 1993).

The earthquake itself and especially catastrophic tsunami waves, generated by the underwater source, caused severe damage on the coast of Okushiri Island and the southwestern coast of Hokkaido. About 330 people were killed (*Furumoto*, 1993) and several hundred houses were completely destroyed. Extensive damage and casualties occurred on Honshu Island; serious damage was also caused in the Primorye Region of Russia and on the Korean coast.

Tsunamis were observed all around the Japan Sea coasts of Japan, Russia and Korea. Especially strong waves occurred on the southwest coast of Okushiri; evidence of 30.6 m tsunami wave run-up was found here by Prof. Y.Tsuji (Earthquake Research Institute, University of Tokyo)*/ .

Several tens of scientists from various countries (Japan, Russia, USA, Korea etc.) are working now on investigation of this tsunami. Some preliminary results were published by *Nakanishi et al.* (1993), *Tanioka et al.* (1993), *Choi et al.* (1993), *Bernard et al.* (1993). Other papers are currently in preparation.

Different aspects of this earthquake and tsunami are inspected in detail. In this study we focused our attention on examination of tsunami tide gauge records on the east coast of Korea.

The Hokkaido Southwest (Okushiri) tsunami was recorded on about 70 tide gauges (Tsuji, personal communication). In particular, in the Republic of Korea this tsunami was observed at 6 stations: Sokcho, Mukho, Ulleungdo, Pohang, Ulsan and Pusan (Fig.1). The analysis of these records is the subject of a two-part study, of which this, the first part, is devoted to estimation of important statistical and spectral characteristics of tsunami waves on the Korean coast and decay of wave energy. The general description of tsunamis in the Sea of Japan observed in this century is presented in section 2. In section 3, observational data of 1993 tsunami and some preliminary data processing are described. Individual tsunami oscillations are examined in section 4 and their essential parameters are estimated. Comparative analysis of energy decay for various stations expounded in section 5 shows that the character of this decay strongly depends on the local topography of the corresponding regions. Section 6 is concerned with spectral analysis of tsunami records and preceding background oscillations performed by means of Fast Fourier Transform. Some principal results of statistical and spectral analysis are discussed in section 7. Cross-spectral analysis tecnique and evolution spectra are used in part 2 to investigate wave structure of this tsunami near the coast of Korea. Observational results are compared with numerical estimates of edge and leaky waves for the examined region (*Rabinovich and Oh*, 1994).

---

*/ E.Bernard and F.Gonzalez estimated tsunami run-up here as 31.5 m (*Gonzalez*, personal communication).

Concentrating our attention on analysis of tsunami records we will not discuss here a question of wave run-up at the Korean coast caused by the Hokkaido Tsunami. Brief preliminary information on this topic was published by *Choi et al.* (1993); and the corresponding full papers are in preparation now. The description of the earthquake itself may be found in the papers by *Nakanishi et al.* (1993) and *Tanioka et al.* (1993).

2. TSUNAMIS IN THE SEA OF JAPAN

The Sea of Japan is not so seismically active as for example deep-sea trenches in the western Pacific (*Koyama and Kosuga,* 1986). In spite of this, at least 20 tsunamis have been recorded in this region (*Tsuji,* 1986; *Chu and Tsuji,* 1993; *Chung et al.,* 1993a). Four tsunamis with magnitude $m > 2$ were observed in the Sea of Japan in this century (Fig.1):

1) Kamuimisaki-Oki (Shakotan) tsunami (August 2, 1940, $M = 7.5$, $m = 2$);

2) Niigata tsunami (May 7, 1964, $M = 7.5$, $m = 2$);

3) Nihonkai-Chubu (Akita) tsunami (May 26, 1983, $M = 7.7$, $m = 2.5$);

4) Hokkaido Southwest (Okushiri) tsunami (July 12, 1993, $M = 7.8$, $m = 3$).

The two last events were the most ruinous tsunamis in Japan in 15 years. The epicenters of all these earthquakes, as well as the epicenters of the Moneron Earthquake, September 6, 1971 ($M = 6.1$, $m = 1$) and the earthquakes on May 1, 1939 ($M = 7.0$, $m = -1$), November 4, 1947 ($M = 7.0$, $m = 1$), May 7, 1964 ($M = 6.9$, $m = 1$) and June 21, 1983 ($M = 7.0$, $m = 0$), were located in the back arc of the Sea of Japan, in the northeastern part of the sea (*Koyama and Kosuga,* 1986; *Tsuji,* 1986). As it is well seen in Fig.1 the Hokkaido Southwest Earthquake occurred just in the gap between the epicenters of the 1940 and 1983 Earthquakes. The Kampo Tsunami, one of the strongest tsunamis in the Sea of Japan (August 29, 1741; $M = 7.5$, $m = 3$) (*Tsuji,* 1986) was caused by an epicenter located practically in the same region.

This information shows that this region was sufficiently active in the last 55 years. Many papers have been published on tsunamis and tsunamigenic earthquakes in this area, especially on the 1983 tsunami (see, for example, *Soloviev and Go*, 1974; *Soloviev*, 1978; *Tsuji et al.*, 1985; *Abe*, 1985; *Kajiura*, 1986; *Soloviev et al.*, 1986; *Abe and Ishii*, 1987; *Chu*, 1987; *Go et al.*, 1988; *Satake et al.* 1988; *Satake and Shimazaki*, 1988a,b; *Abe*, 1990; *Chung et al.*, 1993b, and others).

Practically all tsunamis generated in the Sea of Japan (except the relatively weak Moneron tsunami) were observed on the coast of Korea (*Chu*, 1987; *Chu and Tsuji*, 1993; *Chung et al.*, 1993a). A sad experience of the Chilean tsunami, May 22, 1960 showed that even distant tsunamis may be extremely dangerous, especially for regions with evident resonant topographical features. That is one important reason of the present investigation for the coast of Korea.

3. OBSERVATIONS AND PRELIMINARY ANALYSIS

Tsunami waves propagating from the source area arrived at the mainland coast of Korea in 100-110 min (Fig.2). There are 6 tide gauge stations on the Japan Sea coast of the Republic of Korea (Fig.1) and they all recorded tsunami waves generated by the Hokkaido Southwest Earthquake (Fig.3, 4). The Nichonkai-Chubu tsunami, 1983, was recorded by the same stations (*Chung et al.*, 1993b). These stations may be divided into three groups:

1) Sokcho and Mukho, located in the central part of the east Korean coast where the coastline and continental shelf are relatively straight and smooth;

2) Pohang, Ulsan and Pusan, situated in the southeastern part of the Korean Peninsula, a region with a very complicated coastline, where a number of inlets, bays and islands exert an essential influence on the wave field;

3) Ulleungdo, a small isolated island in the open sea where influence of topography is probably insignificant.

The corresponding tsunami records were fairly similar in Mukho and Sokcho: tsunami waves showed up clearly at these stations; 'ringing' lasted for about 24-28 hours but with fast, obvious decay of wave height; the prominent periods of the observed waves were about 10 minutes; and background oscillations before tsunami arrival were relatively weak, especially in Sokcho (Fig.3).

The records in Pohang, Ulsan and Pusan had more complicated character: tsunami waves at these stations were much weaker and background waves stronger than for the stations of the first group; typical periods of tsunami oscillations were 2-3 times greater and wave height decay was slower (Fig.4).

The Ulleungdo tsunami record was characterized by fast decay, negligibly small background noise before the tsunami, and very short visible periods of tsunami waves (about 5-6 min) (Fig.3).

For further analysis all tide gauge records were carefully digitized and linearly interpolated with a time step of 30 sec. This procedure was made for tsunami waves as well as for background oscillations in the one or two days before the tsunami. The only exception was the Ulleungdo record where background noise was too weak to be analysed; for this reason, only a short length of record, just preceding the tsunami arrival, was digitized for this station.

Tides are weak in the Sea of Japan, except the region of the Korea Strait (in particular, Pusan). But for better detection of tsunami waves and accurate estimation of their statistical characteristics tides were predicted using 6 main tidal constituents for all stations and subtracted from the initial records.

There was a noticeable low frequency drift in the records of Ulsan and Pusan, probably related to the atmospheric processes. This drift was estimated and also subtracted from the records.

To avoid possible distortions of phase and amplitude characteristics of the original tsunami waves, we did not use any kind of high-pass filters in processing the tsunami data.

4. TSUNAMI WAVE STATISTICS AND HISTOGRAMS

Some essential characteristics obtained both from initial and residual series are presented in the Table 1.

First of all, it is interesting to compare computed and actual arrival times of tsunami waves at the Korean stations. The following values were estimated from the Tsunami Travel Time diagram, computed by JMA (Fig.2): 89, 102, 102, 140, 135 and 190 min (the order is the same as in Table 1). The agreement for all stations except Pohang is perfect, especially taking into account the influence of some coastal effects not considered in the model. Pohang is an exception: the leading tsunami wave came to this station 43 min later than expected from the computations; the reason for this strong disagreement is not clear but is probably related to the influence of shallowwater in

Young-il Bay and Pohang New Harbour which are not included in the JMA n model.

The first tsunami wave showed up at the northern stations (Sokcho, Ulleungdo) as a gradual rise in sea level (Fig.3). The fifth wave was the highe Ulleungdo and Mukho (with maximal absolute/relative elevations 89/67 and cm), the second wave was the highest at Sokcho (130/95 cm). Maximal trough wave heights for Mukho, Sokcho and Ulleungdo were about 272, 179, an (Table 1). It is interesting to note that the maximal ebb in Sokcho (-95 observed more than 2.5 hours after the first wave arrival (Fig.3, Table 1).

An ebb (negative) tsunami wave arrived first at the 3 southern station The wave field at these stations was of more complicated character. It is not s distinguish the strongest oscillation for these stations because many wa practically the same amplitudes. Maximal trough-to-crest heights for Pohan and Pusan were 60, 31 and 24 cm (Table 1).

Residual series of tsunami waves were used to distinguish individual os and to estimate their periods and heights (Fig.5-8). The actual tsunami record tsunami sinks into the background signal) had different durations for different The durations of the corresponding segments (in hours) which were used for and construction of histograms are shown in parentheses in Table 1.

It is clear that the observed wave periods varied greatly for different Typical tsunami periods at the Sokcho and Mukho stations were about 10 min, up to 20 min; for the island station Ulleungdo these periods were even smalle 3-6 min, maximal 16 min). Southern stations had greater periods, in particul min in Pusan and 30-35 min in Ulsan; maximal wave periods at these stations 65 min (Fig.5, 7). The general distribution of tsunami wave periods for these was also much wider and had more complicated, nonhomogeneous character, e in Pohang (Fig.7). The change of periods in Pohang with time is interesti increase practically linearly from 8-10 min to 30-40 min (Fig.5).

Typical trough-to-crest wave heights (double the amplitudes) were 15 for Sokcho and Mukho, 30-55 cm for Pohang and 4-20 cm for Ulsan and Pusa 8). The maximum tsunami wave height was observed in Mukho (272.4 c distribution of wave heights agreed relatively well with Rayleigh distributio stations except probably Ulsan (Fig.8).

5. DECAY OF TSUNAMI ENERGY

Munk, Miller, and Snodgrass probably were the first to study tsunami energy decay (*Miller et al.*, 1962; *Munk et al.*, 1962; *Munk*, 1963). Considering the data from the Chilean tsunami May 22, 1960, they found that tsunami variances in the northeastern Pacific decay strictly exponentially in the frequency range 1 to 20 cph:

$$E(t) = E_0 e^{\alpha t} \quad , \qquad (1)$$

where t is time, E_0 is the tsunami energy index, $\alpha = 1/T_0$ is the attenuation coefficient, and T_0 is the "decay" (e-folding) time. The decay time T_0 = 1/2 day was found to be insensitive function to frequency (*Munk et al.*, 1962), although in a previous paper, (*Miller et al.*, 1962), it was postulated that T_0 increases with decreasing frequency and with decreasing energy density. High wave activity in tsunami frequency range was observed for practically a week; the rms amplitudes of the corresponding oscillations reduced by a factor of about 1/e per day.

Van Dorn (1984, 1987) examined decay of tsunami energy in the Pacific for five large tsunamis and and got very similar results except that his estimation of T_0 was 22 hours (Table 2). He found also that expression (1) works perfectly when $t > t_d$, where t_d = 40 h is the "diffusion time" required for the Pacific to become isotropic. Good agreement between different stations and very stable values of T_0 and t_d suggesting a remarkable isotropy in energy density and direction of the energy flux in the mid Pacific ocean.

The same kind of analysis was carried out by *Van Dorn* (1987) in the records of the 1983 Nihonkai-Chubu tsunami at three stations (Fukaura, Toyama and Tonaura) located on the western coast of Honshu in the Sea of Japan. As in the Pacific, after an initial diffusion period, here only about 10 h, the decay rate at all stations was uniformly exponential; the decay time T_0 of 5-hourly consecutive variances was only about 8.6 h, much smaller than in the Pacific (Table 2).

Satake and Shimazaki (1988b) investigated energy decay of the 1964 Niigata and 1983 Nihonkai-Chubu tsunamis at the stations Saigo and Iwasaki (Fukaura), using 5-hour segments of record. They also found that after a small diffusion period (t_d < 5 h) the decay was practically exponential with the averaged value of T_0 = 22.5 h. However they used band-pass filtered records for a band between 50 min and 5 h to eliminate tidal and local resonance effects. The bigger decay time obtained by *Satake and*

Shimazaki (1988b) in comparison with *Van Dorn* (1987) indicates that the attenuation is smaller for the low-frequency tsunami band.

Both *Van Dorn* (1987) and *Satake, Shimazaki* (1988a,b) chosed stations relatively weakly affected by local topographical effects, because they wished to investigate global or, at least, regional tsunami behaviour and energy decay. Here, on other hand, one of the main purposes of the present study is the investigation of local effects.

The decay of local tsunami energy at the Korean coast was examined using tsunami records for all 6 stations. Consecutive 4-hour long pieces of record with moving one-hour (for northern stations) and two-hour (for southern stations) shifts were used to analyse changes of tsunami variances with time. The corresponding results are presented in Fig.9. The station Ulsan was not included in the figure because of low tsunami/background ratio and the confused picture for this station. For all other stations the picture is very clear: fast decay of tsunami energy with time is obvious. At the same time, the significant role of the local topography is quite evident. In particular, the station Ulleungdo, located in the open sea, had the fastest decay; the southern stations situated in nearly enclosed bays and harbours had long 'ringing' and slower decay.

The attenuation coefficients α (per day) were estimated by least-squares fitting of the tsunami variance values (Fig.9). The corresponding decay times T_0 (in hours) were found to be: 3.1 (Ulleungdo), 3.9 (Sokcho), 5.7 (Mukho), 8.5 (Pusan) and 13.3 (Pohang). That means that the 1993 tsunami oscillations at the three northern stations on the Korean coast decayed much faster than was observed by *Van Dorn* (1987) and by *Satake and Shimazaki* (1988b) for the 1983 tsunami on the western coast of Honshu. However T_0 at Pusan was practically the same as obtained by Van Dorn, and at Pohang it was 1.5 times greater. Significant differences in the T_0 values for different stattions prove that the changes of tsunami wave energy with time are related to the Q-factors of the corresponding local domains rather than to characteristics of the source area or to the Q-factor of the Sea of Japan as a whole.

The diffusion period t_d = 4-6 h is clearly seen in Fig.9b for the southern stations. Very small diffusion period or no diffusion were observed at the northern stations (Fig.9a).

Figure 9 shows that distribution of tsunami energy with time at the mainland stations (i.e. except Ulleungdo) is more 'humplike' than linear. These humps are apparently related to the multiple reflection of tsunami waves from the coasts of Korea

and Japan. The greater time differences between the humps for the southern stations (6 - 8h) in comparison with northern ones (4 - 5h) is a response to the greater tsunami propagation time across the Sea of Japan for these stations.

6. SPECTRAL ANALYSIS OF TSUNAMI RECORDS

Spectral analysis of tsunami records is important for estimation of dominant periods and frequency characteristics of tsunami waves, for understanding the resonant influence of the topography of the corresponding region and, probably, for the reconstruction of the tsunami source.

There are several papers on spectral analysis of tsunami records in various regions of the World Ocean (e.g. *Takahasi and Aida,* 1961, 1963; *Miller et al.,* 1962; *Watanabe,* 1964; *Loomis,* 1966; *Miller,* 1972; *Yaroshenja,* 1974; *Sanchez and Farreras,* 1983; *Van Dorn,* 1984; *Soloviev and Kulikov,* 1987; *Baptista et al.,* 1992; *Rabinovich et al.,* 1993; *Gonzalez and Kulikov,* 1993, etc.). Two main results of these works are the following:

(1) Spectra of tsunami records are strongly affected by local topography, i.e. by the continental shelves and resonant features of the corresponding bays and harbors. there fore, tsunamis from different earthquakes have similar spectra at the same location and different spectra for the same event for nearby locations.

(2) The magnitude of the earthquake, the size, location, focal depth, and structure of the source, determine the general spectral energy of tsunami waves and distribution of this energy between different natural periods.

Spectral characteristics of tsunamis in the Sea of Japan were analyzed by *Van Dorn* (1987), *Satake and Shimazaki* (1988 a,b), and *Abe* (1990), using tide gage records from the western coast of Japan. In particular, *Satake and Shimazaki* (1988 a,b) showed that spectral maxima in the frequency range between 0.08 and 0.4 mHz (i.e. for periods 3.5 h - 40 min) for the 1964 Niigata tsunami at this coast were determined mainly by regional resonance oscillations over the shallow water area long the east margin of the Sea of Japan, whereas the 1983 Nihonkai-Chubu tsunami at these periods excited both regional oscillations and free (seiche) oscillations in the Sea of Japan as a whole. This difference is apparently related to the different locations and sea depths of the 1964 and 1983 tsunami sources (about 100 m in the first case and 2500 in the second one.)

Abe (1990) processed tide gauge records of the 1983 tsunami observed at 29 stations on the western coasts of Honshu and Hokkaido and found a strong individuality of the corresponding tsunami spectra. In the same time there were a few common spectral maxima with periods less than 60 min apparently related to the influence of the continental shelf.

In the present study we used the same approach for spectral analysis as was described by *Kovalev et al.* (1991) and *Rabinovich et al.* (1993). Tsunami and background records were processed together for comparative analysis using the Fast Fourier Transform procedure. The records for all five mainland stations were analysed with $T_{t,b}$ = 12.8 h: (1) beginning 16 h before the event ('background spectrum'); (2) during the tsunami ('tsunami spectrum'). The Kaiser-Bessel window (*Harris,* 1978) with length n = 512 (i.e. 256 min) and halfwindow overlapping was performed to improve the spectral estimates. This provided spectral resolution Δf = 0.0039 cpm and degrees of freedom ν = 10. The corresponding values for an island station Ulleungdo, where the actual tsunami was shorter, were: n = 256, Δf = 0.0078 cpm and ν = 12; only the tsunami record (T_t = 7.47 h) was analysed at this station because background oscillations were too weak here. The results of the spectral analyses are presented in Fig.10.

We will describe briefly certain features of the spectra for every station.

Sokcho

At frequencies less than 0.05 cpm (i.e. for periods more than 20 min) spectra are smooth; the background spectrum decreases slowly; the tsunami spectrum for these frequencies is practically equal to constant. At frequencies more than 0.15 cpm both background and tsunami spectra in Sokcho (as well as in all other stations) decrease quickly. There are two not very prominent maxima in the background spectrum with periods about 17 and 13 min. A maximum with period 13 min is evident in the tsunami spectrum; there is also a weaker extremum with period about 8.5 min.

Mukho

The general character of the spectra is similar to those for Sokcho. There are two main maxima in the background spectrum with periods 26-28 min and 13 min. The tsunami spectrum has a relatively broad maximum with periods 12.5-17 min and a sharp spectral peak with period 8.5 min.

Pohang

Pohang harbour is a place well known for strong seiche oscillations even in the absence of tsunamis (*Chu*, 1976). The background spectrum has two broad noticeable maxima with periods 60-85 min and 22-28 min; a weaker maximum has period 8.5 min. The same maxima manifested themselves clearly in the tsunami spectrum. The spectral peak with period 8.5 min increased significantly and looks very similar to that one in Mukho (Fig.10). The main background maximum in the tsunami spectra is divided into two maxima with periods 22.5 and 28 min. *Park et al.* (1986) found very similar periods in the background oscillations in this region, in particular, 60-80 min and 20-25 min.

Ulsan

The background spectrum in Ulsan is relatively smooth except for a broad maximum with a peak period of about 65 min. There are also weaker extrema with periods 32-35 min and 13 min. The main tsunami maximum has period 33 min. Another spectral peak with period 22.5 min can be seen, but the most remarkable feature of the tsunami spectrum is (once again!) a notable maximum with 8.5 min period.

Pusan

The background spectrum in Pusan has three evident peaks with periods 43-50, 21-22, and 16 min. The same peaks occur in the tsunami spectrum; there are also additional maxima with periods 8.5 and 5.5 min.

Ulleungdo

The tsunami spectrum at this station has a few peaks; the most important of them has period 8-9 min. The other noticeable maxima are 15.5, 4.0 and 3.1 min. No maxima appear at low frequencies. It is clear that the main tsunami energy at Ulleungdo is concentrated in the frequency band 0.03 - 0.3 cpm, i.e. at periods 3 - 30 min.

The following preliminary conclusions can be drawn from this analysis:

1) In general, spectra of tsunamis and background have a similar shape but differ by 1-2 (Pusan, Ulsan, Pohang) or 2-3 (Mukho, Sokcho) orders of magnitude.

2) The main maxima for Pusan, Ulsan and Pohang during a tsunami event are the same as in the background spectrum and apparently are related to eigenoscillations of the corresponding basins. In particular, there is a good agreement of observed periods

of spectral maxima in Pohang with the periods theoretically computed by *Park et al.* (1986) for Young-il Bay (70 and 25 min) and Pohang Harbour (22.5 and 7.5 min).

3) There are some differences in observed periods for tsunami and background waves at the stations Sokcho and Mukho. Thus, there is a prominent maximum in the tsunami spectrum with period of about 8.5 min for Mukho which is absent in the background spectrum. The same maximum is observed also in spectra of practically all other stations. Apparently this maximum is related rather to the tsunami source than to the influence of topography.

4) It is clear that the difference between background and tsunami spectra is greater for high frequencies than for low frequencies, probably because of the influence of the tsunami source.

7. DISCUSSION AND CONCLUSIONS

The tsunami July 12, 1993, was clearly manifested at the coast of Korea. Evident differences in the observed periods, wave heights, energy decay, duration of oscillations and other characteristics of tsunami waves at various stations demonstrate distinctly a strong influence of local topography on tsunami behaviour.

The highest waves were observed on the northeastern coast of the Republic of Korea in the region of Mukho station where trough-to-crest heights were up to 2.72 m. Apparently amplification of tsunami waves here was related first of all to the influence of the relatively straight and homogeneous shelf bordering the coastline in this region. In comparison with Ulleungdo, an island station situated in the open sea beyond the shelf, tsunami heights were amplified by factors of 3 at Mukho and 2 at Sokcho, in spite of the greater distance from the source.

It is interesting to compare the tsunami spectra at the coastal stations Mukho, Sokcho with the spectrum in Ulleungdo. The same spectral parameters were used for this computation: $T_t = 7.47$ h, $n = 256$, $\Delta f = 0.0078$ cpm and $\nu = 12$. The corresponding results are presented in Fig.11.

We can assume that the Ulleungdo spectrum (a station scarcely influenced by topography) is sufficiently close (within some constant factor) to the initial tsunami spectrum near the source area. The principal tsunami energy at this station was concentrated at comparatively high frequency, peaking at 0.12 cpm (period 8.5 min).

This means that the initial earthquake displacement was confined to a relatively small area.

The differences of tsunami spectra at Sokcho and Mukho from the spectrum at Ulleungdo can be contributed essentially to the influence of topography, i.e. continental shelf and local bay/harbour effects. As seen in Fig.11, spectra of Ulleungdo and Sokcho are practically coincident at frequencies more than 0.2 cpm, i.e. there are no significant topographical influences affecting the Sokcho spectrum at these frequencies. The Mukho spectrum exceeds (by about half an order of magnitude) the spectrum at Ulleungdo at two high-frequency bands: 0.5-0.7 cpm and 0.23-0.4 cpm. But the main difference between spectra at Sokcho and Mukho and those at Ulleungdo is at low frequencies; at all frequencies below 0.15 cpm, they exceed the Ulleungdo spectrum by 1-1.5 orders of magnitude (Fig.11). Hence the essential topographical amplification of tsunami waves approaching the coast of Korea took place in this frequency band.

Comparative analysis of the island station Ulleungdo and mainland stations give us additional opportunities to investigate the wave structure of tsunami waves. This topic is the subject of the part 2 of this study.

The comparison of tsunami spectra for different stations is important for another reason. No attempts were made to correct tsunami records on unknown filtering effects of tide gauge stilling wells. *Satake et al.* (1988) made a special investigation of these effects at 40 tide gauges on the Japanese coast and found that at some of them (e.g. at Fukaura) the distortion of the tsunami signal was quite noticeable. Good agreement of the high-frequency parts of tsunami spectra for different tide gauges in our case indicate that this effect is not significant for the Korean stations or, at least, that they are distorted in the same way.

The general behaviour of tsunami oscillations at these 3 northern stations (Sokcho, Mukho, and Ulleungdo) was quite similar. The highest waves were observed soon after tsunami arrival (the fifth wave at Ulleungdo and Mukho, the second one in Sokcho). After that the wave heights decreased quickly. The decay times were found to be 3.1 h in Ulleungdo, 3.9 h in Sokcho, and 5.7 h in Mukho.

The character of tsunami oscillations at the three southern stations (Pohang, Ulsan, Pusan) was very different from those at the northern stations. Apparently, the eigenoscillations of local bays and harbours have a major influence. Incoming tsunami waves generated intensive seiche oscillations at these stations, slowly reducing with time. The decay times were 13.3 h in Pohang and 8.5 h in Pusan; the decay time in

Ulsan was difficult to estimate because of the unclear picture of the oscillation station (Fig.4, 6). It was also not easy to determine the strongest oscillation southern stations because many waves were observed with roughly the same hei

The oscillations in Pohang had quite interesting behaviour; their increased practically linearly with time from 8-10 min to 30-40 min (Fig.5). E incoming tsunami waves initially excited here relatively high frequency eige with periods close to the periods of the tsunami source, e.g. the mode in Poha Harbour with period 7.5 min, as computed by *Park et al.* (1986). Later howeve some energy shifted to lower modes or the latter were possibly more lightly d *Park et al.* (1986) computed the period of the fundamental mode in Pohar Harbour to be 22.5 min; the two lowest computed periods for Yong-il Bay (sea Pohang New Harbour) are 70 and 25 min.

Another interesting feature found by tsunami data analysis is clear evid waves reflected from the opposite shore of the Sea of Japan probably fr northwestern coast of Honshu. This result is in a good agreement with results by *and Shimazaki* (1988 a,b) who demonstrated that tsunami sources in the Sea o excite quite effectively the eigenmodes (free oscillations) of the Sea as a whole.

All the results described here were obtained from analysis of the Korean of the 1993 tsunami. It would be interesting to provide a comparison with an results for Japanese and Russian coasts which are much nearer to the source area

ACKNOWLEDGMENTS

This research was supported by the Korea Science and Engineering Foun Project Number 922-27-00-12, and partly by the Korea Institute of Scien Technology. The manuscript was prepared with the support of the Institute of Sciences (IOS), Sidney, B.C., Canada. The authors would like to thank Mr. Ch Park, graduate student of SNU, Seoul, Korea, for the digitizing and preparatior initial data, Dr. R. Falconer Henry (IOS) for his constructive comments on the and Ms. Patricia Kimber (IOS) for her assistance in preparation of the figures.

REFERENCES

Abe, K. (1985). Quantification of major earthquake tsunamis of the Japan Sea. *Phys. Earth Planet. Inter.*, vol.38, p.214-223.

Abe, K. (1990). Spectral characteristics of the 1983 Japan Sea tsunami observed in Japan. *Tohoku Geophys. J.*, vol.32 (2), p.97-106.

Abe, K. and Ishii, H. (1987). Distribution of maximum water levels due to the Japan Sea Tsunami on 26 May 1983. *J. Oceanogr. Soc. Japan,* vol.43, p.169-182.

Baptista, M.A., Miranda, P., and Victor, L.M. (1992). Maximum entropy analysis of Portuguese tsunami data. The tsunamis of 28.02.1969 and 26.05.1975, *Science of Tsunami Hazards,* vol.10 (1), p.9-20.

Bernard, E.N., Gonzalez, F.I., Shuto, N. et al. (1993). Tsunami devasters Japanese coastal region. *EOS*, vol.74 (37), p.417, 432.

Choi, B.H., Kim, Y.B., Ko, J.S., Chung, H.W., Oh, I.S., Choi, J.I., Shim, J.S., and Pelinovsky, E.N. (1993). Tsunami runup survey on eastern Korean coast due to the 1993 Hokkaido Earthquake. *Newsletter of Korean Soc. Coast. Ocean Eng.,* No 93-07, 10 Aug. (in Korean).

Chu, K.S. (1976). The seiches at Pohang Harbour. *J. Oceanol. Soc. Korea,* vol.11 (2), p.51-56 (in Korean).

Chu, K.S. (1987). *On Storm Surges and Tsunami Occurred in the Coast of Korea.* Hydrogr. Office of Korea, 153 p. (in Korean).

Chu, K.S. and Tsuji, Y. (1993). Historical records of earthquakes and tsunamis in the region of the Korean Peninsula and its vicinity. *Proc. IUGG/IOC International Tsunami Symposium,* Wakayama, Japan, p.397-407.

Chung, J.Y., Go, Ch.N. and Kaistrenko, V.M. (1993a). Tsunami hazard estimation for the eastern Korean coast. *Proc. IUGG/IOC International Tsunami Symposium,* Wakayama, Japan, p.409-422.

Chung, J.Y., Kim, S.D. and Ivanov, V.V. (1993b). Tsunami wave forecasting and aposteriori estimation in the East Sea (Japan Sea). *Proc. IUGG/IOC International Tsunami Symposium,* Wakayama, Japan, p.209-221.

Furumoto, A.S. (1993). Three deadly tsunamis in one year. *Science of Tsunami Hazards,* vol.11 (2), p.111-121.

Go, C.N., Kaistrenko, V.M., Pelinovsky, E.N. and Simonov, K.V. (1988). A quantative estimation of tsunami hazard and the tsunami zoning scheme of the Pacific coast of the USSR. *Pacific Annual,* USSR Academy of Sciences, Far Eastern Branch, Vladivostok, p.7-15.

Gonzalez, F.I. and Kulikov, Ye.A. (1993). Tsunami dispersion observed in the deep ocean. *Tsunamis in the World,* ed. by S.Tinti. Kluwer Publ.House, The Netherlands, p.7-16.

Harris, F.J. (1978). On the use of windows for harmonic analysis with the discrete Fourier transform. *Proc. IEEE,* vol.66, p.51-83 (also in: *Modern Spectrum Analysis, II,* ed. by S.B.Kesler, IEEE Press, New York, 1986, p.172-204).

Kajiura, K. (1986). Height distribution of the tsunami generated by the Nihonkai-chubu earthquake. *Science of Tsunami Hazards,* vol.4 (1), p.3-14.

Kovalev, P.D., Rabinovich, A.B., and Shevchenko, G.V. (1991). Investigation of long waves in the tsunami frequency band on the southwestern shelf of Kamchatka. *Natural Hazards,* vol.4, p.141-159.

Koyama, J. and Kosuga, M. (1986). Tsunamegenic earthquakes in the Pacific and the Japan Sea. *Science of Tsunami Hazards,* vol.4 (2), p.83-90.

Loomis, H.G. (1966). Spectral analysis of tsunami records from the stations in the Hawaiian Islands. *Bull. Seismol. Soc. America,* p.697-713.

Miller, G.R. (1972). Relative spectra of tsunamis. Hawaii Inst. Geophys. *HIG-72-8,* Honolulu, 7 p.

Miller, G.R., Munk, W.H., and Snodgrass, F.E. (1962). Long-period waves over California's continental borderland. Part II. Tsunamis. *J. Mar. Res.*, vol.20 (1), p.31-41.

Munk, W.H. (1963). Some comments regarding diffusion and absorption of ıis. Proc. Tsunamis Meeting, 10th Pacific Science Congress, Honolulu, *IUGG ;r.* No 24, p.647-663.

Munk, W.H., Miller, G.R. and Snodgrass F.E. (1962). Long-period waves over rnia's borderland, Part III. The decay of tsunamis and dissipation of tidal energy. : *Res.*, vol.20, p.119-120.

Murty, T.S. (1977). *Seismic Sea Waves - Tsunamis*, Bull. Fish. Res. Board a 198, 337 p.

Nakanishi, I., Kodaira, S., Kobayashi, R. and Kasahara, M. (1993). Quakes and ıis devastate small town. *EOS*, August 24, p.377-379.

Park, H.I., Chung, J.Y. and Oh, I.S. (1986). Numerical experiments of the seiche ıng-il Bay and Pohang New Harbour, Korea. *J. Oceanol. Soc. Korea*, vol.21 (4), 258 (in Korean).

Rabinovich, ,A.B., Djumagaliev, V.A., Fine, I.V. and Kulikov, E.A. (1993). sis of weak tsunamis in the region of Kuril Islands and resonance influence of ·aphy. *Proc. IUGG/IOC International Tsunami Symposium*, Wakayama, Japan, 05.

Rabinovich, A.B. and Oh, I.S. (1994). Manifestation of Hokkaido Southwest hiri) tsunami, 12 July, 1993, at the coast of Korea: 2. Wave structure (in ation).

Sanchez, A.J. and Farreras,. S.F. (1983). Maximum entropy spectral analysis of nis along the Mexican coast,1957-1979. *Tsunamis - Their Science and eering, Proc. International Tsunami Symposium*, Sendai, Japan, p.147-159.

Satake, K., Okada, M. and Abe, K. (1988). Tide gauge response to tsunamis: ırements at 40 tide gauge stations in Japan. *J. Mar. Res.*, vol.46, p.557-571.

Satake, K. and Shimazaki, K. (1988a). Free oscillation of the Japan Sea excited :thquakes. - 1. Observation and wave-theoretical approach. *Geophys. J.*, vol.93 451-456.

Satake, K. and Shimazaki, K. (1988b). Free oscillation of the Japan Sea excited by earthquakes. - II. Modal approach and synthetic tsunamis. *Geophys. J.*, vol.93 (3), p.457-463.

Soloviev, S.L. (1978). Principal data on tsunamis for the Pacific coast of the USSR, 1937-1976. *Tsunami Research in the Open Ocean*, Nauka Publ. House, Moscow, 61-136 (in Russian).

Soloviev, S.L. and Go, C.N. (1974). *Catalogue of Tsunamis on the Western Shore of the Pacific Ocean.* Nauka Publ. House, Moscow, 310 p. (in Russian; English translation in Fish. Aqua. Sci.,1984, Ottawa, Canada, No 5078).

Soloviev, S.L., Go, C.N. and Kim, Kh.S. (1986). *Catalog of Tsunamis in the Pacific, 1969-1982.* USSR Academy of Sciences, Soviet Geophysical Committee, Moscow, 164 p. (in Russian).

Soloviev, S.L. and Kulikov, E.A. (1987). Spectral analysis of mareograms from Urup tsunamis of 13 and 20 October, 1963. *Science of Tsunami Hazards,* vol.5 (1), p.57-63.

Takahasi R. and Aida I. (1961). Studies on the spectrum of tsunami. *Bull. Earthq. Res. Inst.*, vol.39, p.523-535 (in Japanese).

Takahasi R. and Aida I. (1963). Spectra of several tsunamis observed on the coast of Japan. *Bull. Earthq. Res. Inst.*, vol.41, p.299-314 (in Japanese).

Tanioka, Y., Ruff, L., and Satake, K. (1993). Unusual rupture process of the Japan Sea Earthquake. *EOS*, August 24, p.377-380.

Tsuji, Y. (1986). Comparison of observed and numerically calculated heights of the 1983 Japan Sea Tsunami. *Science of Tsunami Hazards*, vol.4 (2), p.91-110.

Tsuji, Y., Baek, W.S., Chu, K.S. and An, H.S. (1985). Report of the Nihonkai-Chubu Earthquake Tsunami along the east coast of Korea. *Rev. Res. Disast. Prev.* 90, 96 p. (in Japanese).

Van Dorn, W.G. (1984). Some tsunami characteristics deducible from tide records. *J. Phys. Oceanogr.*, vol.14, p.353-363.

Van Dorn, W.G. (1987). Tide gauge response to tsunamis II: Other oceans and smaller seas. *J. Phys. Oceanogr.*, vol.17, p.1507-1516.

Watanabe H. (1964). Studies of tsunamis on the Sanriku coast ofNortheastern Honshu in Japan. *Geophys. Mag.*, vol.32 (1), p.120-127.

Yaroshenja, R.A. (1974). A study on natural oscillations in the sea level of Kurile and Kamchatka inlets. *Tsunami Research Symposium*, Wellington, New Zealand, Bull.15 Roy. Soc. New Zealand, p.39-49.

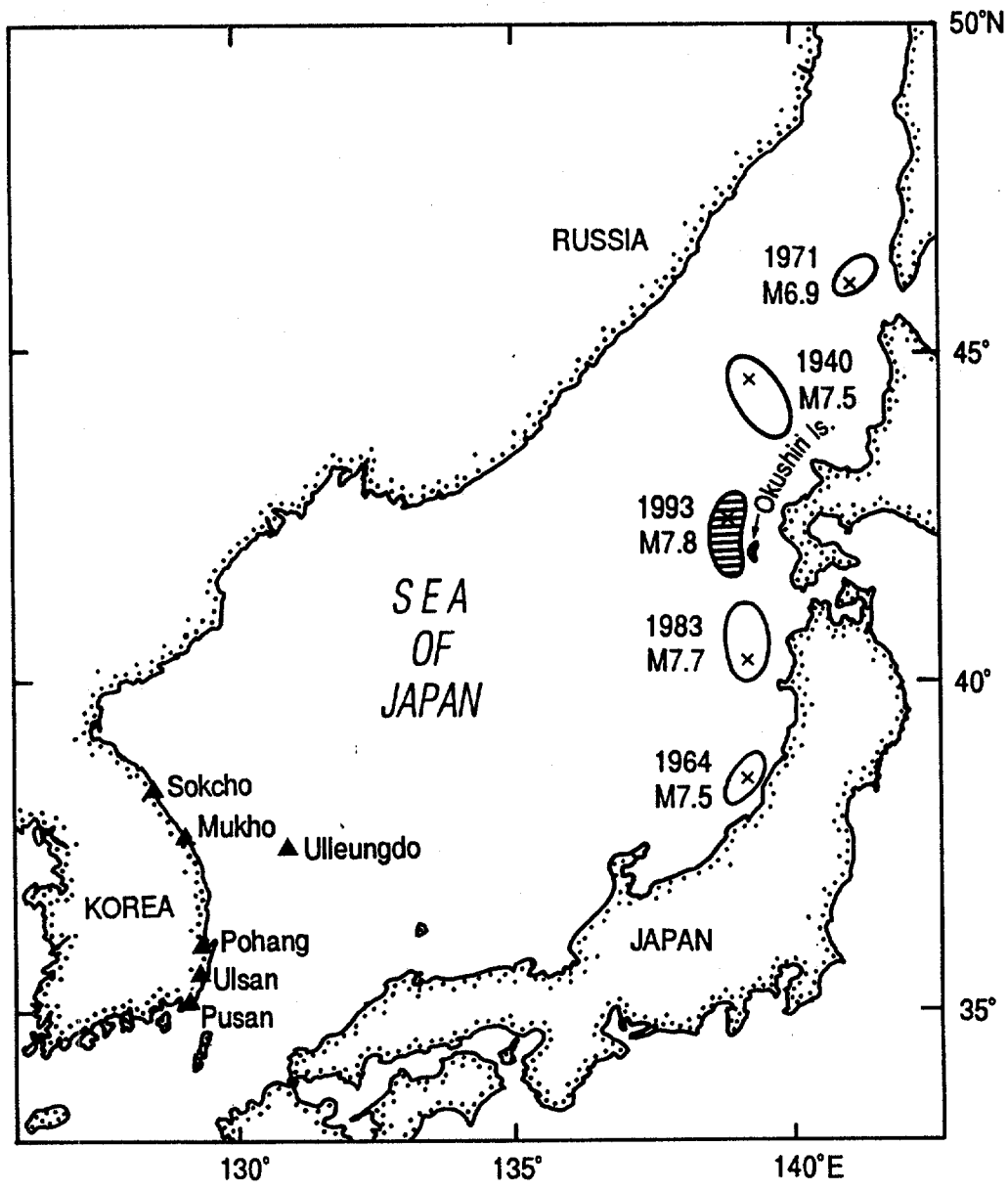

Fig.1. Epicenters of strong 20th century earthquakes in the Sea of Japan. Locations of tide gauges at the coast of Korea are shown.

Table 1. Parameters of the Hokkaido Southwest tsunami waves on the Korean coast

Parameters	Stations					
	Ulleungdo	Sokcho	Mukho	Pohang	Ulsan	Pusan
Arrival time of tsunami waves	12/07 23:46	13/07 00:05	13/07 00:04	13/07 01:20	13/07 00:33	13/07 01:35
Propagation time, min	89	108	107	183	136	198
Maximal absolute elevation						
height, cm	88.5	130.0	212.6	75.0	63.0	104.3
time, hours, min	00:26	00:25	00:53	04:33	02:15	02:38
Maximal relative elevation						
height, cm	67.4	95.3	174.2	46.4	14.3	16.1
time, hours,min	00:26	00:25	00:53	04:33	08:28	07:22
Maximal absolute ebb						
height, cm	-29.5	-60.1	-62.8	-15.0	24.0	44.8
time, hours,min	00:30	02:39	00:31	03:11	06:02	07:41
Maximal relative ebb						
height, cm	-50.6	-95.0	-101.0	-42.6	-17.3	-13.6
time, hours,min	00:30	02:39	00:31	03:12	01:53	06:48
Maximal wave height	93.2	179.2	272.4	59.7	31.4	23.8
Mean wave height, cm	23.6 (8)	45.2 (12)	70.3 (12)	32.9 (18)	14.6 (15)	10.3 (24)
Mean period, min	5.4	10.2	10.2	21.0	29.7	18.5

Comments: (1) Times in the table are in Korean Standard Time (+9 hours relative to GMT).

(2) Absolute values are related to initial tsunami records, relative values are related to residual series after subtracting means, tides and drift.

(3) Time length (in hours) of tsunami segments is presented in parentheses; these segments were used to estimate mean wave heights and periods of tsunami waves, observed at different stations.

(4) Tsunami elevation of 14.1 cm was observed in Ulsan at 02:16.

Table 2. Tsunami energy decay parameters in the Pacific Ocean and the Sea of Japan

Author (s)	Decay time (T_0) (hour)	Diffusion time (t_d) (hour)	Region, Tsunamis
Miller et al. (1962) Munk et al. (1962) Munk (1963)	12	≈ 20	Pacific: Chilean tsunami, May 22, 1960
Van Dorn (1984, 1987)	22	40	Pacific: 5 large tsunamis (1946, 1952, 1957, 1960, 1964)
Van Dorn (1987)	8.6	10	Sea of Japan: Nihonkai-Chubu tsunami, May 26, 1983
Satake and Shimazaki (1988b)*	22.5	< 5	Sea of Japan: Niigata tsunami, May 5, 1964; Nihonkai-Chubu tsunami, May 26, 1983

* For the periods 50-300 min

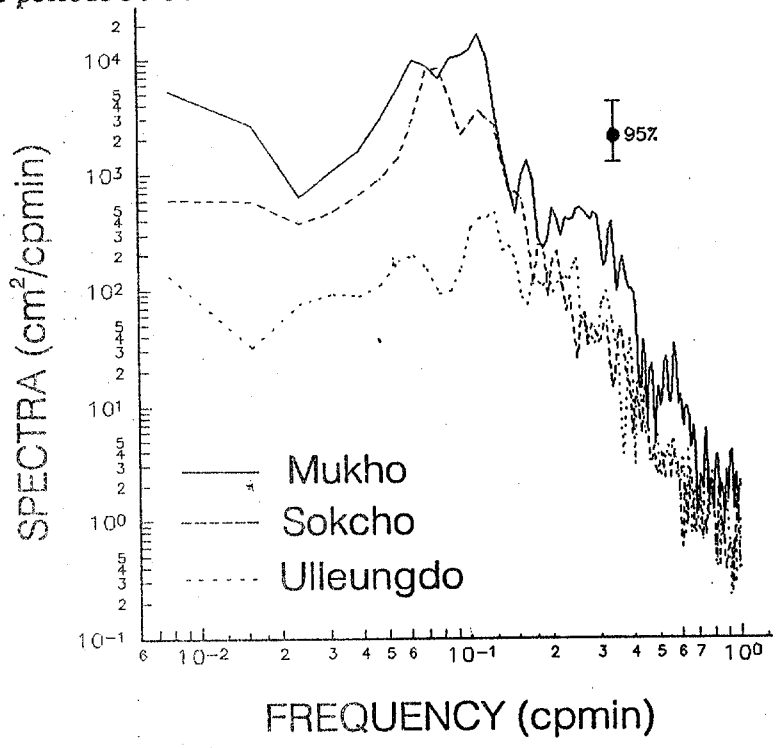

Fig.11. Comparison of 1993 tsunami spectra for three northern stations (continental stations Mukho, Sokcho, and an island station Ulleungdo).

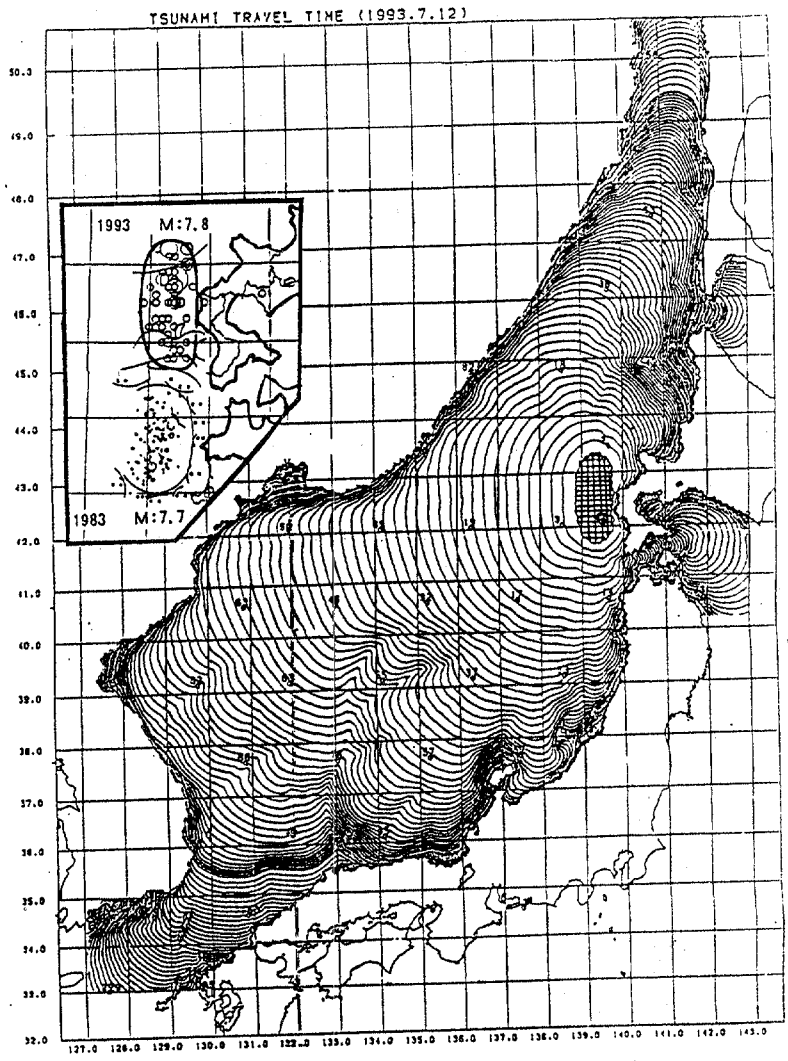

Fig.2. Tsunami travel time computed by Japan Meteorological Agency (JMA) for 1993 Hokkaido Southwest tsunami in the Sea of Japan. Lines are drawn every 2 min up to 120 min, then every 6 min. The epicenters of 1983 and 1993 earthquakes are shown.

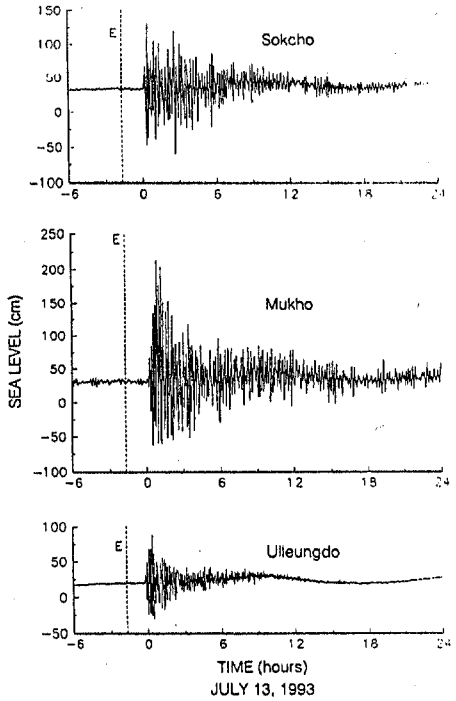

Fig.3. Digitized original tide gauge records at Sokcho, Mukho and Ulleungdo (Korea) for 1993 Hokkaido Southwest tsunami. The time of main shock is marked by E and dashed line.

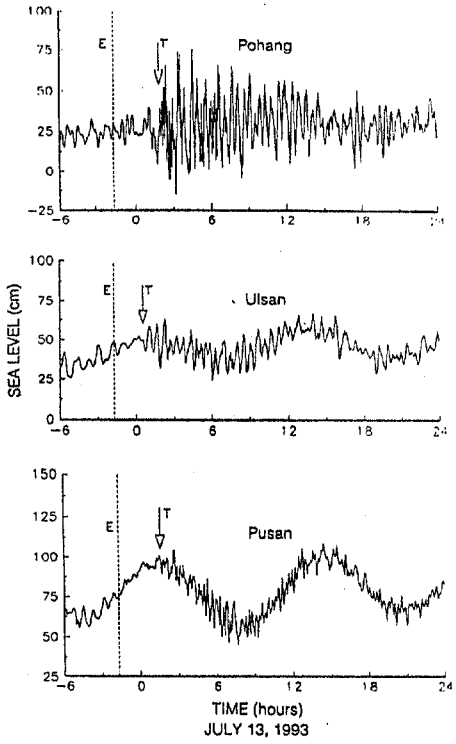

Fig.4. The same as in Fig.3 at Pohang, Ulsan, and Pusan. Tsunami wave arrivals are marked by T and arrows.

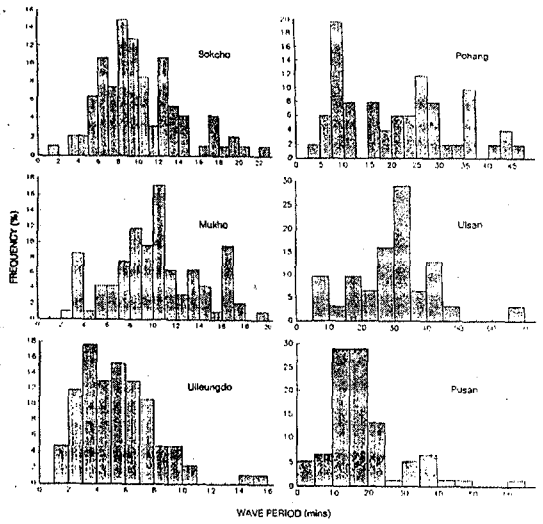

Fig.7. Distribution of periods of tsunami waves.

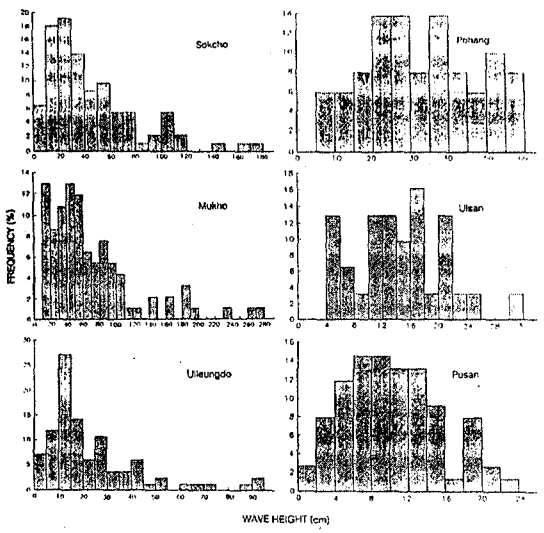

Fig.8. Distribution of tsunami wave heights.

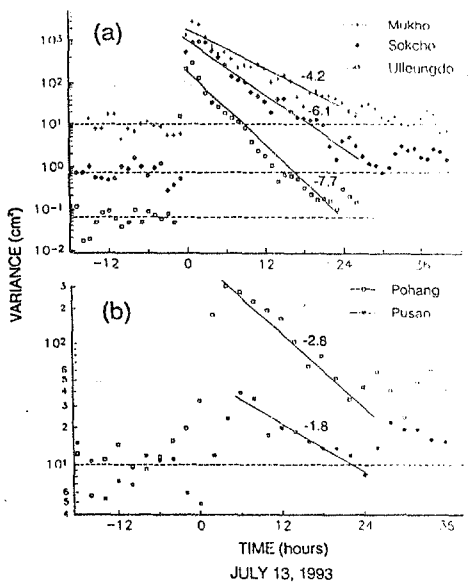

Fig.9. Decay of tsunami energy with time for the northern (a) and southern (b) stations.

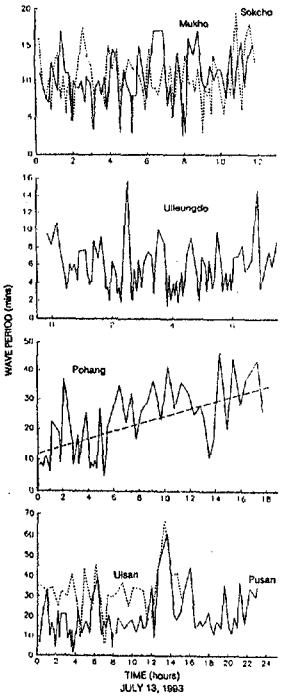

Fig.5. Temporal variations of periods of separate tsunami oscillations at the coast of Korea.

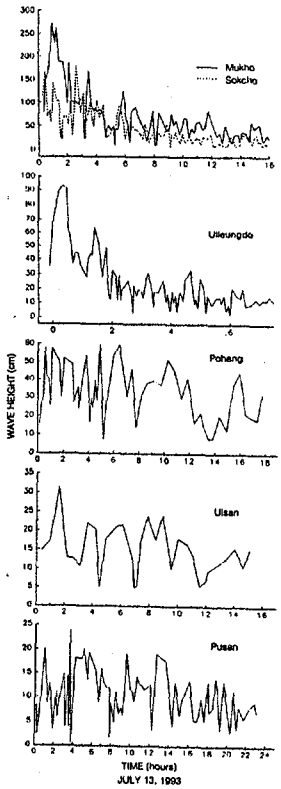

Fig.6. The same as in Fig.5 for wave heights.

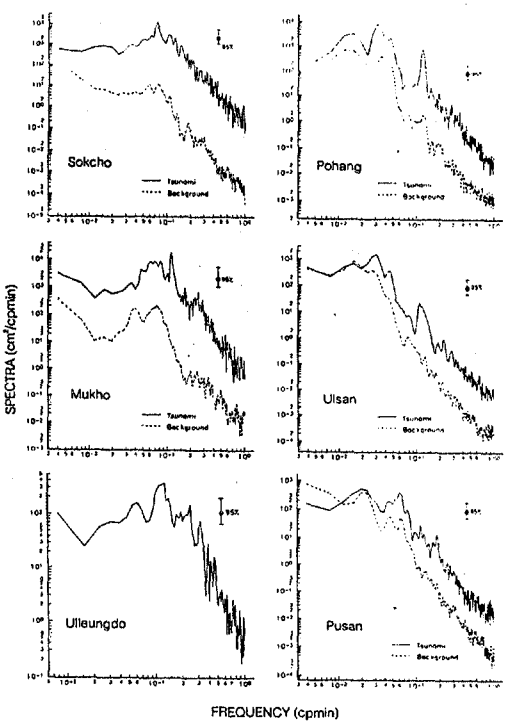

Fig.10. Tsunami and background spectra at the Korean coast for the1993 Hokkaido Southwest tsunami.

REVISED SOURCE OF THE TSUNAMI OF AUGUST 23, 1872

Doak C. Cox
Joint Institute for Marine and Atmospheric Research
University of Hawaii
Honolulu, HI 96822

James F. Lander
Cooperative Institute for Research in Environmental Sciences
University of Colorado
Boulder, CO 80309

ABSTRACT

A recently found marigram recorded at St. Paul Island, one of the Pribilof Islands in the Bering Sea, shows the tsunami that was recorded or observed in Oregon, California, and Hawaii in August 1872. The first manifestation of the tsunami at St. Paul Island was a rise beginning at 20:14 GMT on 23 August. The maximum range of the tsunami waves was 1.5 feet, and the apparent period for the first couple of oscillations 33 or 34 minutes.

A wide variety of sources for the tsunami was suggested by early investigators but Cox (1984) determined from the difference in the tsunami arrival times at San Francisco and Honolulu that it originated on the Pacific shelf and slope of the eastern Aleutian Islands. With the addition of the evidence of the St. Paul Island marigram to the evidence previously available, it appears that the longitude of the center of the source area was between 164° and 171° W, its latitude was between 51° and 54° N, and the origin time of the tsunami was between 17:55 and 18:20 GMT on 23 August. Whether the first feature to reach San Francisco and Honolulu was a crest or a trough is uncertain. If it was a crest, the origin time was most probably about 18:06 GMT and the longitude of the source center was most probably about 168.5° W. If it was a trough, the origin time was most probably about 18:00 GMT and the source center longitude was most probably about 166.4° W-.

There are no known reports of the tsunami or of an accompanying earthquake in the sparcely settled source region.

This is the earliest instrumentally located tsunami source and, most probably, the earliest instrumentally determined earthquake epicenter.

University of Hawaii, Joint Institute for Marine and Atmospheric Research, contribution no. 94-277.

INTRODUCTION

The source or the tsunami of August 1872 was the subject of inquiry almost as soon as the event occurred. It was recorded on marigrams at Astoria, Oregon, and San Francisco and San Diego, California. In Hawaii it was recorded as well as observed at Honolulu on the island of Oahu, and observed at Hanalei and Nawiliwili on the island of Kauai and at Hilo on the island of Hawaii. A variety of generating mechanisms and source areas were suggested by investigators, few of whom were aware of all of the available information on the tsunami. Examples include: a source in the vicinity of the Ryukyu Islands (George Davidson, quoted by Yale, 1872); association with an eruption of Mauna Loa and hence a source in Hawaii (Sapper, 1917, 1927, Jaggar (1931, 1946), Powers (1946); a source near Chichijima in the Bonin Islands (Solov'ev & Go, 1974, 1975); and a meteorological origin or a source "somewhere north of the Hawaiian Islands" (Cox and Morgan, 1977). A more extensive discussion of earlier accounts of the tsunami may be found in the report of Cox (1984), who, taking into account all of the then available data, concluded that the tsunami most probably originated off the Fox Islands in the eastern part of the Aleutian archipelago.

Issuance of this supplementary report is justified by the recent finding of a marigraphic record of the tsunami at Village Cove, St. Paul Island (57° N, 170° W), one of the Pribilof Islands in the Bering Sea.

REPORTS OF THE TSUNAMI IN HAWAII AND ESTIMATION OF ITS HONOLULU ARRIVAL TIME

Although the tsunami was recorded by a tide gage at Honolulu Harbor, the only record of the arrival time that seems to reflect the evidence of the Honolulu marigram is that reported in a newspaper, the Pacific Commercial Advertiser. Hawaii was, at the time, an independent kingdom. The tide gage had only recently been installed when the tsunami arrived, and it was operated for only a few months. The marigrams it produced cannot now be found in Hawaii, and although the originals, tracings from them, or tabular tidal values read from them were sent to the U. S. Coast and Geodetic Survey in Washington, they cannot now be located in the archives of that agency.

In attempting to determine the source of the tsunami, Cox (1984) used an estimate of its arrival time at Honolulu based on several newspaper accounts: 1) that which apparently reflected the arrival time indicated by the tide-gage record; 2) one in the Hawaiian Gazette reporting the time of observation at Honolulu related to the sounding of a noon whistle; and 3) others in the two English-language newspapers reporting times of observation at Hanalei, Nawiliwili and Hilo. An additional account of the tsunami has recently been found in the 29 August issue of Ke Au Okoa, a Hawaiian-language newspaper, and translated into English. The first feature observed at Honolulu was reported in this account to have been a recession beginning at 12:00. The tsunami was described as including three principal early oscillations but as continuing noticeable until evening. The article added that "a man from the lighthouse" reported a 15-inch fall in water level. The Honolulu Harbor lighthouse, which had been erected on piles near the edge of the channel northeast of Sand Island as it then existed, was the site of the tide gage. Hence the 15 inches probably represented the range of the largest fall as recorded by the gage.

The same newspaper article included a report of the observation of the tsunami on Kauai, but with fewer details than had been reported in the English-language newspapers.

. The noon observation of an initial recession had been reported in the Hawaiian Gazette article available to Cox. Hence the information in the Ke Au Okoa article provides no basis for revision of his estimate of the arrival time of the tsunami at Honolulu. The estimate was in the form of a range of values depending on whether the initial feature of the tsunami was a crest or a trough and on whether the reported times of arrival at some of the places were local times or Honolulu times, and, in addition on the differences between the tsunami travel times to the several places in Hawaii and hence the direction of approach of the tsunami to the Islands. Assuming the source to have been on the Aleutian shelf and slope between 164° and 170° W longitude as now estimated, and assuming that the first feature of the tsunami at Honolulu was a crest, as Cox considered probable, his estimate of the probable Honolulu arrival time was between 22:19 and 23:06, and most probably about 22:40 GMT.

INITIAL FEATURE AND ARRIVAL TIME OF THE TSUNAMI AT SAN FRANCISCO AND PREVIOUS ESTIMATION OF ITS SOURCE

Portions of the Astoria, San Francisco, and San Diego marigrams showing the beginning of the tsunami were reproduced in Cox's (1984) report. The beginning cannot be identified with certainty on the Astoria and San Diego marigrams. Hence Cox based his estimation of the tsunami source primarily on the difference between the arrival times of the tsunami at Honolulu and San Francisco. Whether the initial feature at San Francisco was a crest or a trough is not clear from the San Francisco marigram. Listed in Table 1 are both the time of the beginning of the rise to the crest that Cox considered the most probable initial feature and that of the beginning of the fall to the trough that he thought the next most probable initial feature.

Cox concluded that the source area of the tsunami was most probably centered at about 52°N. 170° W, that it was most probably generated at about 18:02 GMT, and that it almost certainly originated off the Aleutian Islands somewhere between 53° N, 165° W and 52° N, 176° W at a time between 18:02 and 18:24 GMT on 23 August.

MARIGRAPHIC RECORD AT ST. PAUL ISLAND

The finding of the St. Paul Island marigram showing the tsunami (Figure 1) was fortuitous. Lander came across it unexpectedly in gathering, from the NOAA National Ocean Survey's archive, copies of marigrams that were related to a project to improve the tsunami database of Alaska. The tide gage had been installed in June 1872 on a pier at Village Cove on the south coast of the island. It ran well through August and intermittently into December when ice destroyed the pier. The marigraphic record had not been requested for use in the project, but the rolls were found in a box with records from a gage operated at Ilinilink, near the eastern end of the Aleutian Islands. (The Ilinilink tide gage was the only one in operation in Alaska earlier than that at St. Paul I., having been installed in November 1871 and operated until January 1872.

The height scale was not indicated on the St. Paul marigrams, but from predicted tide heights supplied by Geoffrey French, NOAA/NOS, a probable reduction of 6:1 was deduced. This scale and chart-time corrections indicated by periodic annotations on the marigrams have

been taken in account in preparing the reproduction of the marigram in Figure 1. The marigram itself is reproduced in Part A of the figure. Part B shows the water-level departures from tide level.

As indicated by Figure 1, continuing seiche activity with periods in the range from a few minutes to about half an hour and with amplitudes up to 0.25 feet is characteristic at Village Cove. However, on August 23 at 09:06 chart time there is very clearly recorded the beginning of the rise to a crest 0.5 feet above normal tide level that is certainly part of the tsunami. Clock corrections of -6.5 minutes at noon on August 22 and -14 minutes at noon on August 23 are indicated on the record. By interpolation, the correction at the time of the beginning of the rise is -13 minutes; the corrected local (170° 16' W meridian) time is 08:53; and, with the 11 hr. 21 min. time difference, the beginning or the rise was at 20:14 GMT.

The maximum range of the departures from tide level, that from the first trough to the succeeding crest, was about 1.5 feet. For the first two major oscillations of the tsunami the apparent period was about 33 or 34 minutes.

RE-ESTIMATION OF TSUNAMI SOURCE

The implications of the marigraphic record of the tsunami arrival at St. Paul Island were investigated through the construction of an inverse tsunami travel-time diagram from the Village Cove site of the tide gage southward across the Bering Sea and through the Aleutian Islands to the general area of the Aleutian shelf and slope in which the previously available information had suggested the source was located. The diagram was constructed manually assuming the applicability of the shallow-water wave velocity using the bathymetric data shown in conventional National Ocean Service charts (principally no. 16382 for the vicinity of St. Paul island, nos. 16011 and 513 for the Bering Sea and parts of the Pacific Ocean adjacent to the Aleutian Islands, and no. 500 for the vicinity of the eastern end of the Aleutian Islands).

That travel-time diagram is the basis for the principal system of isochrones shown in Figure 2. However, in selecting and identifying isochrones for display in the figure, times of travel to or from Village Cove have been replaced by implied Greenwich origin times. For example, the isochrone labeled 18:00 in the figure is that of 2 hr. 24 min. of shallow-water wave travel time to or from Village Cove so that it represents the locus of points on the edge of a tsunami source area from which the front of a tsunami generated at 18:00 GMT would reach Village Cove at 20:24 GMT, the arrival time of the August 27 tsunami suggested by the St. Paul marigram. For brevity, the isochrones based on the tsunami arrival at St. Paul I. will be referred to hereafter as St. Paul isochrones with the respective GMT origin times with which they are identified.

Essentially the same convention will be used in referring to isochrones based on the tsunami arrival at San Francisco and Honolulu that have been added to Figure 2. These isochrones represent parts of the inverse travel-time diagrams for San Francisco and Honolulu that were plotted in Figure 2 of Cox (1984), but with the isochrone labels revised to indicate GMT origin times. Two different origin times are shown for each of the plotted San Francisco isochrones. One was calculated from the time of the beginning of the rise to the crest that Cox considered the most probable initial feature of the tsunami. The other was calculated from the time of the beginning of the fall to the succeeding trough that Cox considered the next most

probable initial feature. Both arrival times are shown in Table 1. To distinguish between the origin times calculated on the two bases the designation "crest" or "trough" will be appended to them in what follows. The arrival time at Honolulu shown in Table 1 and assumed in calculating the arrival times indicated for the Honolulu isochrones is the time considered most probable by Cox (1984) if the longitude of the source were between 160° and 170° W.

If there were no error in estimating either the arrival times of the tsunami at the three places or the travel times from them, the St. Paul Island, San Francisco, and Honolulu isochrones representing the actual origin time of the tsunami should be tangent to the perimeter of the source area. To investigate the range of possible source areas, a number of examples were plotted on the equivalent of Figure 2. Each was assumed to be elliptical, but the areas represented a range of locations, sizes, and orientations, and propagation of the tsunami through the Aleutian islands via several alternative channels or combinations of channels. Two of these examples are shown in Figure 2 and described in Table 2. That the sizes of these examples are reasonable is indicated by the finding by Wells and Coppersmith (1994) of moment magnitudes of earthquakes (approximately equal to surface-wave magnitudes) of 7.4 and 7.7 or 7.8 correlated with a rupture lengths of 100 km and 200 km, respectively.

It will be noted that it was from the northwestern edge of a source area that the tsunami would propagate toward St. Paul Island but from the southeastern edge that it would propagate toward both San Francisco and Honolulu. Although the initial feature of the tsunami at all three places was considered most probably a crest, Honolulu origin-time isochrones suggested by tangency to ellipses A and B in Figure 2 are tangent to their southeast edges whereas the St. Paul Island equivalents are tangent to their northwest edges. The general experience, in Japan at least, is that, if the initial feature of a tsunami propagating from one side of an elliptical source area is a crest, the initial feature propagating from the opposite side is a trough. Hence, although some of the examples of possible source ellipses, including ellipse A, were plotted so that the San Francisco isochrones tangential to them were "crest" isochrones, others, including ellipse B, were plotted so that the San Francisco isochrones tangential to them were "trough" isochrones. If the initial feature at San Francisco were a trough, the initial feature at Honolulu was also probably a trough. However, the uncertainty of the time of arrival of the tsunami at Honolulu is so great that no distinction was made between "crest" and "trough" Honolulu isochrones.

More important than the variety of origin areas of the tsunami that would be consistent with its estimated arrival times at St. Paul Island, San Francisco, and Honolulu and its estimated travel times to those places are the limits to the origin-area locations suggested by the same data taking limits to the reliability of the estimates into account.

It is quite unlikely that the actual arrival time at St. Paul Island differs from the estimated time by more than about a minute, but there may be greater errors in the estimates of tsunami travel time between the island and possible source areas south of the Aleutian Islands. The distances are short, but the extent of shallow water and irregularities in the bathymetry along the travel path, particularly in the vicinity of the Aleutians and the channels between them, make travel time estimation uncertain. Hence it seems possible that the origin times implied by the St. Paul isochrones in the general area of the source might be in error by 5 or 6 minutes.

Although the distances involved are much greater, errors much greater than 5 minutes are unlikely to result from the use of the hybrid method used by Cox (1984) in estimating travel times between the probable source area and either San Francisco and Honolulu. There is no reason to regard estimates of the arrival time of the tsunami at San Francisco as subject to an uncertainty of more than about a minute other than that stemming from the uncertainty whether initial feature was a crest or the succeeding trough. Hence origin times implied by the San Francisco isochrones in the general area of the source may be considered to be in error by no more than about 7 minutes. The arrival time of the tsunami at Honolulu is much more uncertain, however, and the origin times implied by the Honolulu isochrones in the general area of the source should be considered subject to an uncertainty of at least 15 minutes.

If the origin times implied by both the St. Paul isochrones and the San Francisco (crest) isochrones were either earlier or later than those indicated in Figure 2 by, say, 5 minutes, the origin times associated with origin area A would be 5 minutes earlier or later, respectively than that shown in Table 2. If the origin times implied by the St Paul isochrones were earlier than indicated whereas those implied by the San Franciso (crest) isochrones were later than indicated, the equivalent of origin area A would be shifted westward or southwestward. The limits to the uncertainty of the origin times implied by those isochrones are such, however, that the equivalent to ellipse A could not be shifted so that the longitude of its center were farther west than about 171° W. A shift eastward would result if the changes to the origin times implied by the two sets of isochrones were in the opposite direction. In addition, if the origin times implied by the St. Paul isochrones were later than those shown by 5 minutes, those implied by the San Francisco (crest) isochrones were earlier than those shown by 5 minutes, and those implied by the Honolulu isochrones were later than those shown by 15 minutes, they would be consistent with an origin at about 18:05 on the shelf southeast of the Krenitzin Is. and south of Unimak I. The St. Paul and San Francisco (crest) isochrones would be consistent with a origin as late as 18:15 in the vicinity of the Kretizen Is. themselves, and , considering the uncertainty in the Honolulu arrival time, even an origin this late in this vicinity cannot be ruled out.

Shifts in origin time or location similar to those described for ellipse A would result in the case of ellipse B if it were the trough that was the initial feature at San Francisco, the possible shift of the center eastward being limited to a longitude of about 164° W.

SUMMARY OF CONCLUSIONS

In summary, the August 1872 tsunami was certainly generated off the Pacific coast of the Aleutian Islands as found earlier by Cox (1984). The marigraphic evidence of its arrival at St. Paul Island recently discovered by Lander permits the time and location of its origin to be identified with greater certainty and precision than was possible earlier. Assuming the initial feature of the tsunami propagating southeastward to have been a crest, as considered most likely, its most probable origin time is now estimated at about 18:06 GMT on 23 August, 12 minutes earlier than the time estimated by Cox, and the most probable position of the center of its origin area is now estimated at about 52.2° W, 168.5° W, about 85 km east of the most probable position estimated by Cox. If the initial feature propagating southeastward was a trough, the origin time was most probably about 18:00 GMT, and the center of the origin area was most probably about 53.3° N, 166.4° W. The range of possible origin times, estimated by Cox at 48

minutes (17:36 to 18:24 GMT) is now considered no greater than about 25 minutes (17:55 to 18:20 GMT). The range of possible longitudes of the center of the origin area, estimated by Cox at 11° (165° W to 176°) is now considered no greater than about 7° (164° W to 171° W).

INITIAL FEATURE OF THE TSUNAMI ON THE WEST COAST AND IN HAWAII

In the light of the uncertainty whether the first feature of the 1872 tsunami on the West Coast and in Hawaii was a crest or a trough, the identification of the first feature of other tsunamis with similar source areas is of some interest.

The marigraphic records of the 1946 and 1957 tsunamis that originated off the Aleutian Islands and of the 1964 tsunami that originated in the Gulf of Alaska all show crests as the features arriving first at places on the West Coast and in Hawaii. The intensities of the 1872 tsunami resembled more closely those of the March 1929 tsunami that accompanied a magnitude 7.5 earthquake occurring in the vicinity of the Fox Islands. The 1929 tsunami was recorded at Honolulu and San Francisco (Lander et al., 1993) and also at Hilo, but, as in the case of the 1872 tsunami, there is no record of its observation in Alaska. No attempt seems to have been made to determine its source area from its arrival times in California and Hawaii. However, the location estimated for epicenter of the earthquake it accompanied, 50.9° N, 169.7° W (Stover and Coffman, 1993), when considered in the light of the limited precision of epicenter locations at that early date, suggests that the tsunami source area was similar to that of the 1872 tsunami. The first feature of the 1929 tsunami cannot be identified with certainty on either the San Francisco or Honolulu marigrams, but the first feature recorded at Hilo was clearly a crest.

Hence, the 1872 tsunami seems anomalous if its first feature at places on the West Coast and Hawaii was a crest.

ACKNOWLEDGMENTS

Geoffrey French, NOAA National Ocean Service, supplied an estimate of tide heights at Village Cove, St Paul Island that permitted estimation of the height scale of the marigram on which the August 1872 tsunami was recorded.

The article in Ke Au Okoa referred to in the discussion of reports of the tsunami in Hawaii was found and translated into English by Anthony Keeling, a student of Hawaiian at the University of Hawaii, with the advice of his professor, Emily Hawkins. Keeling's work was supported by the National Science Foundation under BCS 9208173 as, in part, were the restudy of the source of the August 1872 tsunami generally and the preparation of this report.

REFERENCES

Coan, Titus, 1872. Recent eruption of Mauna Loa. Am. J. Sci, ser. 3, vol. 2, no. 23, pp. 406-407.

Cox, D. C., 1984. Probable Aleutian source of the tsunami observed in August 1872 in Hawaii, Oregon, and California, Science of Tsunami Hazards, vol. 2, no. 2, pp. 79-94.

Cox, D. C., and J. Morgan, 1977-78. Local Tsunamis and Possible Local Tsunamis in Hawaii. Univ. Hawaii, Hawaii Inst. Geophys., HIG-77-14, 118 pp. (Nov. 1977); Supplement, 6 pp. (1978).

Jaggar, T. A., 1931. Hawaiian damage from tidal waves. Hawaiian Volc. Obs., Volcano Letter, no. 321, pp. 1-3.Jaggar, T. A., 1946. The great tidal wave of 1946. Nat. Hist., vol. 55, no. 6, pp. 263-268.

Lander, J. F., P. A. Lockridge, and M. J. Kozuch, 1993. Tsunamis Affecting the West Coast of the United States, 1806-1992. NOAA National Geophysical Data Center Key to Geophysical Records Doc. No. 29, 242 pp.

Powers, H. A. The tidal wave of April 1, 1946, in the Hawaiian Islands. Hawaiian Volc. Obs. Volcano Letter, no. 491, pp. 1-4.

Sapper, 1917. Katalog der geslichflichten Vulkansoütbruch, Trübner, Strassbourg.

Sapper, K., T., 1927. Vulcankunde. J. Engelhorn, Stuttgart, 424 pp.

Solov'ev, S. L., and Ch. N. Go, 1974. Katalog Tsunami na Zapdnom Poberezje Tiego Oceana (Tsunamis Occurring on Western Coasts of the Pacific Ocean), Akad. NAUK, USSR, 310 pp. Canadian Translation of Fisheries and Aquatic Sciences 5078, 1984.

Solov'ev, S. L., and Ch. N. Go, 1975. Katalog Tsunami na Vostocnom Poberezje Tiego Oceana (Tsunamis Occurring on Western Coasts of the Pacific Ocean), Akad. NAUK, USSR, 310 pp. Canadian Translation of Fisheries and Aquatic Sciences 5077, 1984.

Stover, C. W., and J. L. Coffman, 1993. Seismicity of the United States, 1568-1989 (Revised). U. S. Geological Survey Prof. Paper 1527, 418 pp.

Wells, D, L, and K. J. Coppersmith, 1994. New empirical relationships among magnitude, rupture length, rupture area, and surface displacement. Bull. Seismol. Soc. Amer., vol. 84, no. 4, pp. 974-1002.

Yale, C. G., (Secretary), 1872. Proceedings, Regular Meeting of October the 7th, 1872. Proc. California Acad. Sci., ser. 1, vol. 4, pp. 267-269.

Table 1. Estimated arrival times of the 27 August 1872 tsunami.

Place	Assumed initial feature	Arrival time, GMT
Village Cove, St. Paul I.	Crest	Aug 23, 20:24
San Francisco	Crest	Aug 24, 00:21
" "	Trough	Aug 24, 00:46
Honolulu	Crest (?)	Aug 24, 22:40

Table 2. Examples of possible origin areas of the tsunami of 27 August 1872.

Possible source area	Channel through Aleutian Is.	Assumed first feature propagating SE	Origin time, GMT	Major axis orientation	Major axis length	Minor axis length	Latitude	Longitude
A	W of Umnak	Crest	18:06	N 42° E	115 km	45 km	52.2° N	168.5° W
B	E of Unalaska	Trough	18:00	N 56° E	195 km	84 km	53.3 ° N	166.4° W

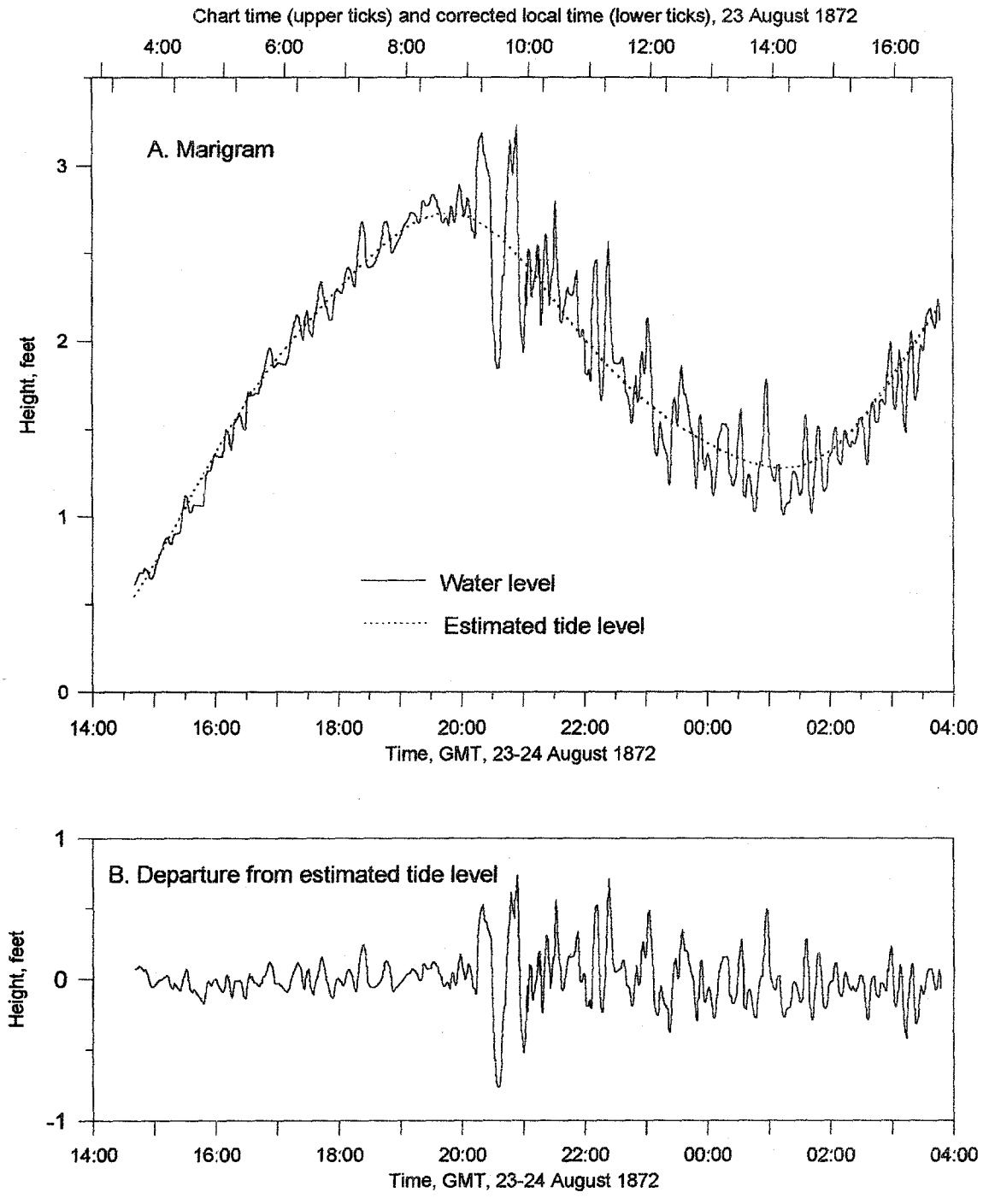

Figure 1. Marigraphic record of arrival of tsunami of 23 August 1872 at Village Cove, St. Paul Island, Pribilof Islands.

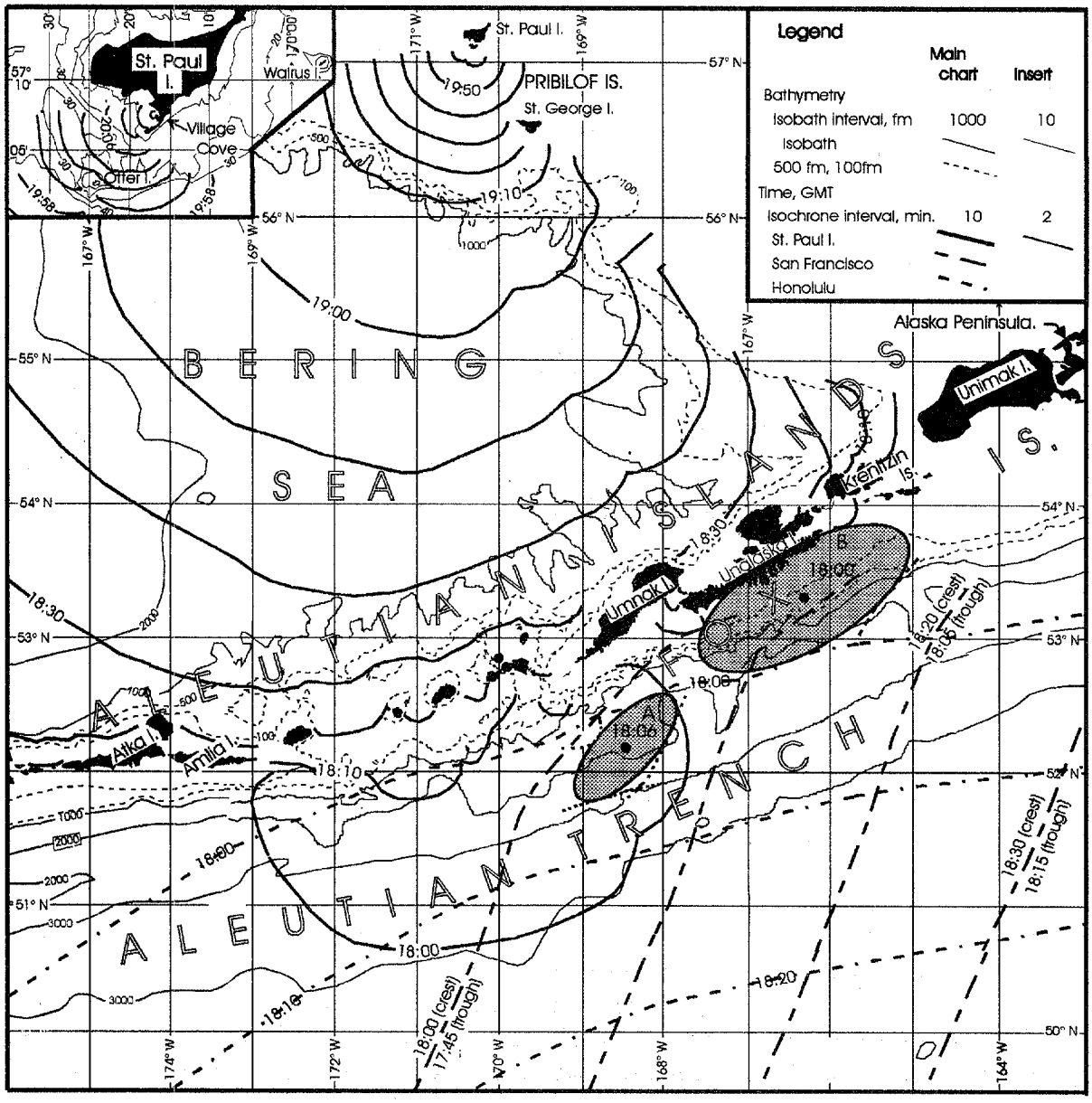

Figure 2. Travel-time chart for August 1872 tsunami in the area from the Pribilof Islands to the eastern Aleutian Islands and the Aleutian Trench.

SPECIAL ANNOUNCEMENTS

The Tsunami Society and the Editor of the *Science of Tsunami Hazards* have NEW ADDRESSES!

THE TSUNAMI SOCIETY
P. O. Box 25218
Honolulu, Hawaii 96825, USA

Dr. Charles L. Mader, Editor
SCIENCE of TSUNAMI HAZARDS
Mader Consulting Co.
1049 Kamehame Drive
Honolulu, Hawaii 96825, USA

IAPSO SYMPOSIUM PS-05 PROGRAM
August 5-12, 1995, Honolulu, Hawaii

The International Association for the Physical Sciences of the Ocean (IAPSO) General Assemby will be held August 5-12, 1995 at the Hilton Hawaiian Village, Honolulu, Hawaii.

As stated by IUGG President Moritz on October 17, 1994, "IAPSO's Assembly and program planned for Hawaii is completely authorized, and I want it to be the best possible."

The theme of IAPSO Symposium PS-05 follows is of interest to Society members.

"This symposium will focus on the circulations and processes in the coastal oceans, especially those having connections or interactions with the land. Problems of estuaries, studies of natural hazards in the coastal zone including storms and TSUNAMIS, and presentations on the mitigation of these hazards will be included."

Tsunami papers should address terminal effects, e.g., coastal flooding and hazards, protection, and other mitigation measures. The abstract deadline for the IAPSO General Assembly is January 31, 1995. For additional information contact Dr. Fred E. Camfield, Corresponding Lead Convenor, IAPSO Symposium PS-05, U. S. Army Engineering Waterways Experiment Station, 3909 Halls Ferry Road, Vicksburg, MS 39180-6199.

Corrections to Volume 12, Number 1

The dates on page 62 should read "1930 - 1994".

An addition to the acknowledgments on page 35. "Partial support was supplied under JIMAR cooperative agreement NA 37RJ0199."

APPLICATION FOR MEMBERSHIP

THE TSUNAMI SOCIETY
P. O. Box 25218
Honolulu, Hawaii 96825, USA

I desire admission into the Tsunami Society as: (Check appropriate box.)

☐ Student ☐ Member ☐ Institutional Member

Name _____ Signature _____

Address _____ Phone No. _____

_____

Zip Code _____ Country _____

Employed by _____

Address _____

Title of your position _____

FEE: Student $5.00 Member $25.00 Institution $100.00

Fee includes a subscription to the society journal: SCIENCE OF TSUNAMI HAZARDS.

Send dues for one year with application. Membership shall date from 1 January of the year in which the applicant joins. Membership of an applicant applying on or after October 1 will begin with 1 January of the succeeding calendar year and his first dues payment will be applied to that year.